

D9.3 - CUTTING-EDGE, EVOLUTIVE, SELF-SENSING AND MULTI-FUNCTIONAL MATERIALS AND TECHNOLOGIES FOR IMPROVING THE RESILIENCE OF BUILDINGS, INCLUDING CULTURAL HERITAGE - DEVELOPMENT FOR THE APPLICATION TO REAL DEMO

September 2025 | KTH

MULTICLIMACT

D9.3 - CUTTING-EDGE, EVOLUTIVE, SELF-SENSING AND MULTI-FUNCTIONAL MATERIALS AND TECHNOLOGIES FOR IMPROVING THE RESILIENCE OF BUILDINGS, INCLUDING CULTURAL HERITAGE - DEVELOPMENT FOR THE APPLICATION TO REAL DEMO

Project Title	MULTI-faceted CLIMate adaptation ACTions to improve resilience, preparedness and responsiveness of the built environment against multiple hazards at multiple scales
Project Acronym	MULTICLIMACT
Contract Number	101123538
Project Coordinator	Rina Consulting S.p.A.
WP Leader:	UNIVPM
Deliverable	D9.3 - Cutting-edge, evolutive, self-sensing and multi-functional materials and technologies for improving the resilience of buildings, including cultural heritage - development for the application to real demo
DoA	Task 9.3 - Materials and technologies for improving the resilience of buildings, including cultural heritage - development for the application to a real demo case [

	development for the application to real demo
DoA	Task 9.3 - Materials and technologies for improving the resilience of buildings, including cultural heritage - development for the application to a real demo case [
Lead beneficiary	КТН
Main Authors	Youssef Elomari (KTH), Qian Wang (Uponor)
Main contributors	Alessandra Mobili (UNIVPM), Gloria Cosoli (UNIVPM), Francesca Tittarelli (UNIVPM), Chiara Giosuè (UNIVPM), Gian Marco Revel (UNIVPM), Youssef Elomari (KTH), Qian Wang (Uponor), Patrizia Aversa (ENEA), Valeria Leggieri (UNICAM), Michele Morici (UNICAM)
Reviewers	Abril Martín (NATURALEA), Alessandra Mobili (UNIVPM), Gloria Cosoli (UNIVPM), Francesca Tittarelli (UNIVPM), Sabrina Hafdhallah (RINA-C), Celina Solari (RINA-C)
Due date	30.09.2025
Report date	17/09/2025
Version	2.0

Document classification

PU Public



WILLIAM (((O

REVISION TABLE

Version	Date	What
1.0	11/07/2025	First draft with complete contributions from UNIVPM side
1.1	23/07/2025	First draft with complete contributions from KTH side
1.2	23/07/2025	First draft with complete contributions from Uponor side
1.3	25/07/2025	First draft including the first round of revisions by UNIVPM
1.4	29/07/2025	First draft incorporating the first round of UNIVPM revisions by KTH
1.5	08/08/2025	Document including revisions by NATURALEA
1.6	29/08/2025	Pre-final version aligned with MULTICLIMACT template and submitted to RINA-C for quality check by KTH
2.0	17/09/2025	Final version ready for submission

Copyright Notices ©2023-2027 MULTICLIMACT Consortium Partners. All rights reserved.

MULTICLIMACT is a Horizon Europe project supported by the European Commission under grant agreement No 101123538.

Views and opinions expressed are however those of the author(s) only and do not necessarily reflect those of the European Union. Neither the European Union nor the granting authority can be held responsible for them.

All information in this deliverable may not be copied or duplicated in whole or part by any means without express prior agreement in writing by the MULTICLIMACT partners. All trademarks and other rights on third party products mentioned in this document are acknowledged and owned by the respective holders.

The MULTICLIMACT consortium does not guarantee that any information contained herein is error-free, or up to date, nor makes warranties, express, implied, or statutory, by publishing this document.



TABLE OF CONTENTS

REVISION	I TABLE	3
EXECUTIV	/E SUMMARY	10
1. IN	NTRODUCTION	11
1.1.	OBJECTIVES AND OUTCOMES	11
1.2.	STRUCTURE OF THE DELIVERABLE	11
1.3.	CONTRIBUTIONS OF PARTNERS	11
2. D	EVELOPMENT OF AN INNOVATIVE HVAC SYSTEM FOR THE DEMONSTRATION SITE OF	RIGA
MARKET		13
2.1.	DESIGN OF LOWTEMPERATURE HEATING SOLUTIONS	13
2.1.1.	UNDER FLOOR HEATING SYSTEM DESIGN	14
2.1.2.	BILL OF QUANTITIES	16
2.2.	MANIFOLD PERFORMANCE ASSESSMENT	22
2.2.1.	CIRCUIT SURFACE TEMPERATURE ANALYSIS	22
2.2.2.	. HEAT OUTPUT DISTRIBUTION ANALYSIS	24
2.2.3.	. CIRCUIT PRESSURE DROP ANALYSIS	24
2.2.4.	. SUPPLY, RETURN AND Δ T PROFILES PER CIRCUIT	25
3. R	ENEWABLE ENERGY-BASED HVAC SOLUTION DEVELOPMENT FOR THE DEMONSTRATION	N SITE
OF RIGA I	MARKET	27
3.1.	BACKGROUND AND CONTEXT	27
3.2.	RIGA MARKET DESCRIPTION	27
3.2.1.	BUILDING THERMAL BALANCE	30
3.3.	PROPOSED RENEWABLE-ENERGY-BASED HVAC CONCEPT	31
3.4.	RESILIENCE ASSESSMENT	34
3.4.1.	COLD-WAVE SCENARIO ANALYSIS	34
3.4.2	. HEAT-WAVE SCENARIO ANALYSIS	36
	EVELOPMENT OF SENSORIZED CEMENTITIOUS BLOCKS FOR STRUCTURAL HIRING PURPOSES	EALTH 38
4.1.	CASTING OF SENSORIZED BLOCKS	38
4.1.1.	CASTING PROCEDURE	39
4.2.	LABORATORY TESTS	46
4.3.	PREPARATION OF THE ITALIAN PILOT	49

5.	DEVELOPMENT OF MULTIFUNCTIONAL	MORTAR	PANELS	FOR	INDOOR	AIR	QUALITY
IMPR	DVEMENT						53
5.1.	OPTIMIZATION OF THE MULTILAYER PA	ANELS					53
5.2	LABORATORY TESTS						55
5.3	PREPARATION OF THE ITALIAN PILOT						64
6.	DEVIATIONS TO THE PLAN						67
7.	OUTPUTS FOR OTHER WPS						68
8.	CONCLUSION						69
9.	LITERATURE /REFERENCES						70

LIST OF TABLES

- TABLE 1. CONTRIBUTIONS OF PARTNERS. 1
- TABLE 2 KEY MANIFOLD CIRCUIT PARAMETERS 16
- TABLE 3. MIX DESIGN OF THE MORTAR FOR SENSORIZED BLOCKS. 45
- TABLE 4. MIX-DESIGN AND WORKABILITY OF RASANTE PER LHP MORTAR IN G/L. 54
- TABLE 5. R_C AND E_D VALUES OF MAPETHERM AR1 GG, RASOBUILD ECO EXTRAFINO, RASANTE PER LHP, AND UNIVPM MORTARS . 56

63

22

- TABLE 6. F_U VALUES OF THE 4 MULTILAYER SYSTEMS. 57
- TABLE 7. FLOW VALUE AND R_c OF THE ORIGINAL AND MODIFIED UNIVPM MORTAR MIX.

LIST OF FIGURES

- FIGURE 1: UPONOR CLASSIC WET UNDERFLOOR-HEATING 14
- FIGURE 2:SINGLE LINE DIAGRAM OF THE UNDERFLOOR HEATING SOLUTION 15
- FIGURE 3:UNDERFLOOR HEATING MANIFOLD WITH VARIO ACTUATORS AND UPONOR SMATRIX CONTROLS
- FIGURE 4: SURFACE TEMPERATURE PER CIRCUIT BY MANIFOLD (M1–M7) 23
- FIGURE 5: HEAT OUTPUT DISTRIBUTION PER CIRCUIT BY MANIFOLD 24
- FIGURE 6:TOTAL PRESSURE LOSS ΔP PER CIRCUIT BY MANIFOLD 25
- FIGURE 7: SUPPLY/RETURN TEMPERATURE AND ΔT PER CIRCUIT BY MANIFOLD 26
- FIGURE 8: THE SELECTED PILOT FOR LTH IN MULTILCIMACT EXISTING BUILDING (TOP) AND IFC MODEL (BOTTOM) [CREDITS: RIGA MUNICIPALITY] 28
- FIGURE 9:HEATING UNIT CONCEPTUAL DIAGRAM [CREDITS: RIGA MUNICIPALITY] 29
- FIGURE 10: TEMPERATURE REGIME IN DH NETWORK (SECOND GENERATION DISTRICT HEATING "2ND GDH") [CREDITS: RIGA MUNICIPALITY] 29
- FIGURE 11: MONTHLY HEATING AND COOLING ENERGY BALANCE [CREDITS: RIGA MUNICIPALITY] 30
- FIGURE 12: SIMPLIFIED SCHEMATIC OF THE INTEGRATED DHN HP BIPV LTH/HTC DISTRIBUTION SYSTEM 31
- FIGURE 13: MONTHLY PV PRODUCTION 65 KWP BIPV SYSTEM 32
- FIGURE 14: COMPARISON OF DESIGNED VS. SIMULATED HEAT OUTPUT PER CIRCUIT ACROSS UFH MANIFOLDS 33
- FIGURE 15: INDOOR AND OUTDOOR TEMPERATURE PROFILES DURING COLD-WAVE SCENARIO WITH PREHEAT OFFSETS (1–5 H) 35
- FIGURE 16: INDOOR AND OUTDOOR TEMPERATURE PROFILES DURING HEAT-WAVE SCENARIO WITH PRECOOL OFFSETS (1–5 H)
- FIGURE 17 DRAWING OF THE WOODEN PANELS USED TO REALIZE THE MOULDS. DIMENSIONS ARE REPORTED IN MM (PICTURE COURTESY OF UNIVPM). 39
- FIGURE 18 SCHEME OF THE WOODEN MOULD ASSEMBLY (PICTURE COURTESY OF UNIVPM). 39
- FIGURE 19 CONNECTION BETWEEN REBAR AND WIRE FOR THE FREE CORROSION POTENTIAL MEASUREMENT (PICTURE COURTESY OF UNIVPM). 40
- FIGURE 20 PROTECTION OF REBAR EXTREMITIES THROUGH THE APPLICATION OF A TWO-COMPONENT RESIN (PICTURE COURTESY OF UNIVPM). 40
- FIGURE 21 ELECTRODES WITHIN THE 3D-PRINTED CASE AND RELATED CABLES (PICTURE COURTESY OF UNIVPM). 41
- FIGURE 22 EXPERIMENTAL SETUP OF CONNECTION BETWEEN ELECTRODE ARRAY AND ACQUISITION BOARD (PICTURE COURTESY OF UNIVPM). 41
- FIGURE 23 MOULD WITH PVC TUBES AND POLYSTYRENE PIECES (PICTURE COURTESY OF UNIVPM). 42
- FIGURE 24 POSITIONING OF STEEL REBARS WITHIN THE MOULD (PICTURE COURTESY OF UNIVPM). 42
- FIGURE 25 MOULD WITH ELECTRODE ARRAY, TIMMO ELECTRODE, AND STEEL REBARS (PICTURE COURTESY OF UNIVPM).

 42
- FIGURE 26 INSTALLATION SCHEME OF SENSORS IN THE CEMENTITIOUS BEAM (PICTURE COURTESY OF UNIVPM). 43
- FIGURE 27 TIMMO PSEUDO-REFERENCE ELECTRODE. 43
- FIGURE 28 CO.S.MO.NET MONITORING SYSTEM (PICTURE COURTESY OF UNIVPM). 44
- FIGURE 29. SCHEME OF THE CONNECTION OF THE STM32 NUCLEO-G491REBOARD FOR ACQUISITION OF FREE CORROSION POTENTIAL (PICTURE COURTESY OF UNIVPM).
- FIGURE 30 SPECIMEN JUST AFTER THE POURING PHASE (PICTURES COURTESY OF UNIVPM). 45



- FIGURE 31. MECHANICAL STRENGTH OF THE INNOVATIVE SELF-SENSING MORTAR DURING THE CURING PERIOD (PICTURES COURTESY OF UNIVPM). 46
- FIGURE 32. ELECTRICAL IMPEDANCE MODULUS AND PHASE OF THE FIRST ECCS BLOCK IN THE LIS' PLATFORM (PICTURES COURTESY OF UNIVPM). 47
- FIGURE 33. ELECTRICAL IMPEDANCE MODULUS AND PHASE OF THE SECOND ECCS BLOCK IN THE LIS' PLATFORM (PICTURES COURTESY OF UNIVPM). 48
- FIGURE 34. FREE CORROSION POTENTIAL OF THE EMBEDDED REBAR OF THE FIRST ECCS BLOCK IN THE LIS' PLATFORM (PICTURE COURTESY OF UNIVPM). 48
- FIGURE 35. FREE CORROSION POTENTIAL OF THE EMBEDDED REBAR OF THE SECOND ECCS BLOCK IN THE LIS' PLATFORM (PICTURE COURTESY OF UNIVPM). 49
- FIGURE 36. GOOGLE MAPS VIEW OF THE LOCATION OF THE ITALIAN DEMO. 50
- FIGURE 37. FAÇADE VIEW OF THE TWO TWIN ROOMS CHOSEN FOR THE ITALIAN PILOT IN THE EX-CARMELITANE BUILDING (PICTURES COURTESY OF UNICAM). 51
- FIGURE 38. PLAN OF THE FIRST FLOOR OF THE EX-CARMELITANE BUILDING (PICTURES COURTESY OF UNIVPM). 51
 FIGURE 39. RECESS OPENED IN THE EXISTING WALL WITH ECCS BLOCKS ON THE FLOOR (PICTURES COURTESY OF UNIVPM).
- FIGURE 40. THE FOUR TESTED MULTILAYER PANEL COMBINATIONS (PICTURES COURTESY OF UNIVPM). 55
- FIGURE 41. FAILURE MECHANISMS OF XPS+PAINT (PICTURES COURTESY OF UNIVPM). 56
- FIGURE 42. FAILURE MECHANISMS OF XPS+UNIVPM (PICTURES COURTESY OF UNIVPM). 56
- FIGURE 43. FAILURE MECHANISMS OF HEMP+PAINT (PICTURES COURTESY OF UNIVPM). 57
- FIGURE 44. FAILURE MECHANISMS OF HEMP+UNIVPM (PICTURE COURTESY OF UNIVPM). 57
- FIGURE 45. WATER VAPOR DIFFUSION RESISTANCE FACTOR (μ) OF THE FOUR MULTILAYER PANELS (PICTURE COURTESY OF UNIVPM). 58
- FIGURE 46. CHANGE IN WATER CONTENT OF THE FOUR MULTILAYER PANELS DURING THE CYCLIC EXPOSURE AT RH = 75% FOR 8 H AND AT RH = 33% FOR 16 H IN THE CLIMATIC CHAMBER (PICTURE COURTESY OF UNIVPM). 59
- FIGURE 47. MBV OF THE FOUR MULTILAYER PANELS (PICTURE COURTESY OF UNIVPM). 59
- FIGURE 48. VOCS CONCENTRATION (%) INSIDE THE BOX WITH THE FOUR MULTILAYER PANELS (PICTURE COURTESY OF UNIVPM). 61
- FIGURE 49. VOCS ADSORPTION (%) OF THE FOUR MULTILAYER PANELS (PICTURE COURTESY OF UNIVPM). 61
- FIGURE 50. NO, NOX AND NO2 DEGRADATIONS INSIDE THE BOX UNDER VIS LIGHT (PICTURE COURTESY OF UNIVPM).
- FIGURE 51. NO, NOX AND NO $_2$ DEGRADATIONS INSIDE THE BOX UNDER UV LIGHT (PICTURE COURTESY OF UNIVPM).
- FIGURE 52. CRACKS DEVELOPMENT ON THE UNIVPM MORTAR APPLIED ON THE MULTILAYER NATURAL-BASED SYSTEM (PICTURE COURTESY OF UNIVPM). 63
- FIGURE 53. VISUAL ASPECT OF MORTARS APPLIED ON NATURAL-BASED PANEL AND SUBSTRATE AFTER 28 DAYS OF CURING (PICTURE COURTESY OF UNIVPM). 64
- FIGURE 54. SCHEME OF POSITIONING OF THE DIFFERENT INNOVATIVE/REFERENCE SYSTEMS (PICTURE COURTESY OF UNIVPM).

 66

Abbreviations and Acronyms

ACRONYM	DESCRIPTION		
всн	Biochar		
ВІМ	Building Information Model		
BIPV	Building-Integrated Photovoltaic		
BOQ	Bill of Quantities		
CE	Counter Electrode		
CEL	Cellulose		
СНР	Combined Heat and Power		
Co.S.Mo.Net	Concrete Structures Monitoring Network		
DH	District Heating		
ECCs	Engineered Cementitious Composites		
EVOH	Ethyl Vinyl Alcohol		
HVAC	Heating, Ventilation and Air Conditioning		
HP	Heat Pump		
нтс	High Temperature Cooling		
IFC	Industry Foundation Classes		
KWp	Kilowatt peak		
κ	Kelvin		
IAQ	Indoor Air Quality		
LHP	Lime Hemp Panel		
LTH	Low Temperature Heating		
MAPE	Mean Absolute Percentage Error		
MLC	Multi-Layer Composite		
MBV	Moisture Buffering Value		
NOx	Nitrogen Oxides		
PE	Polyethylene		
PE-Xa	Cross-linked Polyethylene		
PVC	Polyvinyl Chloride		
PEX	Cross-linked Polyethylene		
RCFs	Recycled Carbon Fibres		

RE	Reference Electrode
RH	Relative Humidity
SE	Sensing Electrode
SHM	Structural Health Monitoring
SP	Superplasticizer
Т	Temperature
TiMMO	Titanium activated with Mixed Metal Oxides
TPU	Thermoplastic Polyurethane
TRL	Technology Readiness Level
UFH	Underfloor Heating
UV	Ultraviolet
VIS	Visible
VOCs	Volatile Organic Compounds
WE	Working Electrode
XPS	Extruded polystyrene
Δρ	Pressure Drop
ΔΤ	Temperature Differential

Executive Summary

The deliverable D9.3 "Materials and technologies for improving the resilience of buildings, including cultural heritage - development for the application to a real demo case" reports the further development of materials for building envelopes and technological equipment that have been designed in T3.3. This further advancement is paramount for testing all the developed solutions in real contexts in two different demo cases, i.e., the Italian and the Latvian demo sites.

In details, UNIVPM self-sensing materials and related sensors for the measurement of electrical impedance have been further developed for the Italian demo. Engineered cementitious composites (ECCs) have been produced with embedded sensors (free corrosion potential measuring electrode and 3D-printed electrical impedance array) and tested in laboratory conditions for monitoring purposes. Also, the UNIVPM multifunctional mortar based on recycled and sustainable materials have been further developed and tested in terms of depolluting and thermo-hygrometric properties by comparing its behavior against petrochemical origin materials. The two solutions will be then further tested, deployed on site and monitored within the framework of T11.1 and T15.1.

For the Latvian demo site, KTH and Uponor jointly led the development of an integrated low-temperature heating system tailored to the Riga Central Market. Uponor designed the preliminary system architecture, including underfloor heating circuit layouts, manifold specifications, and the full bill of quantities. This design will serve as the basis for a new BIM model. Contributed with comprehensive energy and resilience analyses, including thermal balance assessments and dynamic simulations under extreme weather scenarios (cold waves and heat waves). The main work carried out by KTH and Uponor focused on defining a future-proof, renewable-based HVAC concept built around five key components: a building-integrated photovoltaic system, a reversible heat pump, the district heating network, a low-temperature substation, and a combined low-temperature heating/high-temperature cooling distribution system using the Uponor underfloor heating network. The developed technologies will be further refined and validated within the frameworks of T11.4 (Develop and test phases), and T15.4 (Demonstration phases) of the MULTICLIMACT project.

1. INTRODUCTION

1.1. OBJECTIVES AND OUTCOMES

Enhancing the resilience of buildings is fundamental in times when climate change consequences are well evident. Developing innovative solutions to regularly monitor the overall status of buildings allows to have regular information exploitable for management purposes, prioritizing interventions and timely act during eventual emergencies (e.g., seismic events). Also, providing data on the physiological and stress status of the occupants is very relevant in situations that can be dangerous for health and safety, such as heat waves or earthquakes.

This deliverable D9.3 "Cutting-edge, evolutive, self-sensing and multi-functional materials and technologies for improving the resilience of buildings, including cultural heritage - development for the application to real demo", is part of WP9, entitled "Materials and Technologies for supporting the built environment preparedness and responsiveness to disrupting events - Develop". It corresponds to the project's second year, within its development phase, and aims to create resilient materials and technologies to support the MULTICLIMACT action in the built environment, across different scales and contexts, with direct application at the building level.

In this Task, the following solutions have been developed:

- Measurement and real-time monitoring system (in close collaboration with LIS partner) for ECCs with self-sensing materials for SHM, including sensors to measure electrical impedance and free corrosion potential (UNIVPM);
- Innovative multifunctional mortar applied to natural-based thermal insulation panels, designed to improve occupants' health and well-being by reducing indoor pollution, and compared against existing commercial solutions (UNIVPM);
- Innovative HVAC systems, according to the specifications of Riga municipality (KTH, UPONOR).

1.2. STRUCTURE OF THE DELIVERABLE

The Deliverable is structured as follows:

- Section 1 reports the introduction chapter, the objectives and outcomes of Task 9.3;
- Section 2 describes the work carried out for the development of the innovative HVAC system to be deployed in the Latvian demo;
- Section 3 reports the development of the renewable energy-based HVAC system for the demonstration in the Latvian demo;
- Section 4 describes the production and testing at lab scale of ECCs with self-sensing materials and embedded sensors for the Italian demo;
- Section 5 describes the further development and testing at lab scale of the multifunctional mortar;
- Section 6 reports the deviations to the planned activities;
- Section 7 gives the outputs for other WPs related to the T9.3, and
- Section 8 provides the conclusions of the work done. Finally, the document closes with the references of technical works.

1.3. CONTRIBUTIONS OF PARTNERS

The following Table 1 depicts the main contributions from project partners in the development of this deliverable.

Table 1. Contributions of Partners.

PARTN**E**R SHORT NAME

CONTRIBUTIONS



UNIVPM	Overall content to sections 4 and 5, contribution to sections 1, 7, and 8.
ктн	Overall content to sections 2 and 3, contribution to sections 1, 7, and 8.
UPONOR	Overall content to sections 2 and 3, contribution to sections 1, 7, and 8.

2. DEVELOPMENT OF AN INNOVATIVE HVAC SYSTEM FOR THE DEMONSTRATION SITE OF RIGA MARKET

2.1. DESIGN OF LOW TEMPERATURE HEATING SOLUTIONS

This Task involved the design of the preliminary low-temperature heating system for the Riga central market pavilion (i.e., Latvian demo). Energy audit results and data pre-processing confirmed that the pilot is a district-heated cultural-heritage building supplied by a centralized district-heating network. Five heat exchangers with a total installed capacity of 3379 kW serve the complex energy system. During the design phase, several radiant heating systems were assessed through detailed modelling, considering site-specific constraints such as the structural limits of existing materials, shop layouts, architectural preservation requirements, and floor-space restrictions. To meet the heritage floor build-up and embedding-depth limitations, Uponor's Classic wet underfloor-heating system (Figure 1) was selected. Prefabricated, corrosion-protected steel-mesh mats clip directly onto the existing insulation, preserving the historic substrate. Uponor Comfort Pipe PLUS Blue is the state-of-the-art sustainable piping solution using renewable materials with an oxygen diffusion barrier. This barrier consists of a layer of ethyl vinyl alcohol (EVOH) extruded on the outside of the Cross-linked Polyethylene (PEX) pipe. The outermost layer is polyethylene (PE). This layer is very flexible and does not affect the flexibility and pliability of the basic pipe. Renewable PE raw material for the pipe is based on the Bornewables™ product range supplied by Borealis (Vienna, Austria, https://www.borealisgroup.com). These raw materials are made using sustainably sourced renewable feedstocks derived solely from waste and residue vegetable oils, such as used cooking oil and residues from vegetable oil processing. The residue from vegetable oil processing consists of rancid fat that must be removed to produce food-grade oil. The used cooking oil, entirely waste and residues in origin, is a waste stream collected from restaurants and the food industry. The waste and residue raw materials that are used to produce our feedstock are no longer fit for human consumption, and as such, do not impact food security. For MULTICLIMACT, 20 × 2.0 mm dimensions are selected and enables continuous circuit lengths up to 120 m without intermediate joints, efficiently covering large floor areas. The modular design accommodates any insulation material—from standard residential to heavy-duty commercial-without compromising integrity. Comfort Pipe PLUS BLUE is stress-resistant and engineered for long service life, ensuring reliable, low-maintenance performance in a cultural-heritage environment.



Figure 1: Uponor Classic Wet Underfloor-Heating [Credits: Uponor]

Below there are the design and calculation results for the under-floor heating system, including detailed system drawings and a preliminary bill of materials. These results will form the basis of the upcoming tender process to select the installation contractor. They will also serve as the foundation of the new BIM model, with the pipe layout to be installed in accordance with this design. Most of the materials listed in the current bill of quantities will be carried over into the new BIM. Please note that this is a preliminary bill of materials; a fully detailed and precise version will be produced once the new BIM model is complete, since some components cannot yet be quantified at this stage.

2.1.1. UNDER FLOOR HEATING SYSTEM DESIGN

Figure 2 shows the single-line diagram superimposed on the floor plan. Return water from the district-heating network (42-46 °C) enters a low-temperature substation where it is tempered to a 39 °C supply. From there, a main loop circulates at 37745 kg/h through seven manifold stations (M.01-M.07) before returning at 33.8 °C. Each manifold feeds 15-19 individual circuits of (20 × 2.0 mm) Comfort Pipe PLUS, maintaining continuous loop lengths for efficient heat delivery. Available pressure head on the main loop is 111.5 kPa, while individual manifold Δp values range from 66.8 kPa at M.06 to 90.0 kPa at M.05. Isolation valves, flow meters, and differential-pressure gauges at each manifold ensure balanced hydraulics and streamline commissioning.



Figure 2:Single line diagram of the underfloor heating solution [Credits: Uponor]

Table 2 summarizes, for each manifold station (M.01-M.07), the number of circuits, required versus delivered heat outputs, design ΔT (5.0-5.3 K), mass flow (4845-6207 kg/h), pressure drop (55.6-90.0 kPa) and total loop length (1450-1893 m). These data confirm that every circuit stays within the Comfort Pipe PLUS continuous-loop limits while reliably meeting the calculated thermal loads.

Source/Source: 1				: Heating			M edi	um: Wa	ter	
Temperatures θs,H and θr,H	1 [°C]	242	coma, c	39.0		33.8	В			
Temperature source for	control circuits	Source/	1							
Temperatures 0s,H and 0r,H Required heating output Φr Obtained heating output ΦH Heat capacity lost ΦOS,H [\ Mass flow rate m [kg/h]	eq,H [W] H [W]		20	39.0 9532 7643 2837 887.5		33.8	3			
Manifold symbol	Storey symbol	Number of heating/cooling circuits	Obtained output of heat./cool. zone (heating mode)	Output lost of heat./cool. zone (heating mode)	Return temperature on manifold (heating mode)	Temperature difference on manifold (heating mode)	Mass flow rate	Required min. pressure difference	Resultant pressure difference	Total pipe length in loop systems
Manifold	Stor.	N	ФH	ΦOS,H W	θr,H °C	Д θН К	m kg/h	∆pmin kPa	Δp kPa	Ltot
M.01	0	18	32365	1996	33.7		5784.6	68.7	79.2	1801.9
M.02	0	19	33640	2083	33.9	5.1	6207.3	74.0	82.7	1893.3
M.03	0	15	26337	1594	33.9	5.1	4753.3	55.6	71.4	1455.4
M.04	0	18	28991	1828	34.0	5.0	5509.6	64.1	68.0	1698.5
M.05	0	15	27986	1729	33.7	5.3	4972.4	59.5	90.0	1532.2
M.06	0	18	31066	1919	33.9	5.1	5673.2	66.8	66.8	1774.3
M.07	0	16	27259	1687	33.9	5.1	4845.6	58.1	69.6	1520.8

Table 2 key manifold circuit parameters

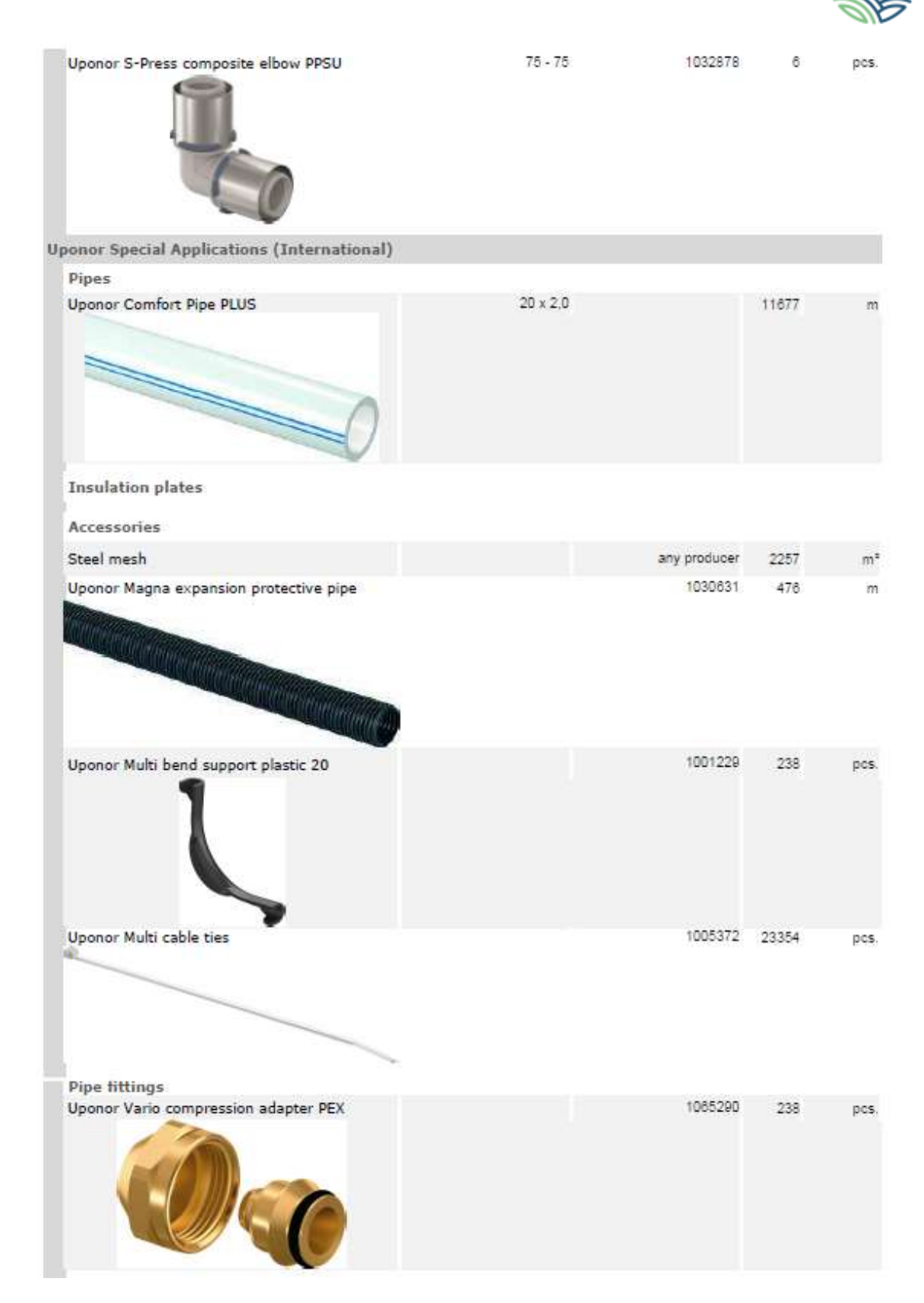
2.1.2. BILL OF QUANTITIES

The bill of quantities (BOQ) specifies all Uponor components required for the Classic wet under-floor-heating installation. It includes: 11677 m of $20 \times 2.0 \text{ mm}$ Comfort Pipe PLUS PE-Xa loops and 2.257 m^2 of corrosion-protected steel-mesh mats in 50 mm, 100 mm and 150 mm grid patterns; seven complete manifold assemblies paired with 416 m of Multi-Layer Composite (MLC) distribution piping; and 476 m of Magna expansion-protective pipe to accommodate thermal movement. In addition, the BOQ provides 23554 master-clips, cable ties and screed accessories to secure the circuits, plus dedicated mounting brackets for each manifold. Below is the full breakdown of BOQ items. Please note that this is a preliminary bill of materials; a fully detailed and precise version will be produced once the new BIM model is complete, since some components cannot yet be quantified at this stage.

Product	Size	Catalogue code	Qty.	Unit
Brass and steel pipe couplings and fittings				
Pipe fittings				
Female connector, reduction, imperial	2"FT - 1%"FT		12	pcs
Female connector, reduction, imperial	2½°FT - 2°FT		2	pcs
Nipple, reduction, imperial	2"MT - 1½"MT		2	pcs
Nipple, straight, imperial	1%"MT - 1%"MT		12	pcs
JPONOR S-Press PLUS PPSU (International)				
Pipes				
Uponor MLC pipe white S, straight lenghts 5m	63 x 6.0	1013451	169	n
Uponor MLC pipe white S, straight lenghts 5m	75 x 7.5	1013453	18	n
Uponor MLC pipe white S, straight lenghts 5m	90 x 8.5	1013455	97	n
Uponor MLC pipe white S, straight lenghts 5m	110 x 10.0	1013457	132	n

				-,-
Pipe fittings				
Uponor RS 2 adapter S-Press	RS 2 - 63	1029125	12	pcs.
Uponor RS 2 adapter S-Press	RS 2 - 75	1029128	2	pcs.
Uponor RS 3 adapter male thread	RS 3 - R3	1029133	2	pcs.
Uponor RS 3 adapter S-Press	RS 3 - 110	1029128	76	pcs.
Uponor RS 3 adapter S-Press	RS 3 - 90	1029127	84	pcs.
Uponor RS 3 coupling	RS 3	1029145	38	pcs.
Uponor RS 3 elbow	RS 3	1029139	24	pcs.

Uponor RS 3 tee	RS 3	1029143	12	pcs.
Uponor RS 3/RS 2 reducer	RS3	1029148	14	pcs
Uponor S-Press adapter male thread	63 - 2 MT	1032895	12	pcs.
Uponor S-Press adapter male thread	75 - 2½°MT	1032896	2	pcs
Uponor S-Press composite coupling PPSU	63 - 63	1032881	:17:	pcs.
Uponor S-Press composite elbow PPSU	63 - 63	1032877	32	pcs.



Manifolds				
Uponor Magna manifold bracket kit		1045816	14	pcs.
Uponor Magna manifold G 11/2-3/4 w. valve	1 out.	1121532	2	pcs.
Uponor Magna manifold G 11:-3/4 w. valve	3 out.	1121534	30	pcs.
Uponor Magna manifold kit		1045815	7	pcs.
Manifold cabinets Uponor Magna cabinet on-wall	1910x835x200mm	1060554	3	pcs.
Uponor Magna cabinet on-wall	2310x835x200mm	1060555	4	pes
Valves Uponor SPI Magna ball valve , set	40	1030135	7	set
Special of Principle Dall Valve / Set	7W 2			961

At position A (Figure 3), the manifold feeds multiple underfloor heating circuits, each regulated by a Vario Actuator NC FT 24 V (Uponor GmbH, based in Haßfurt, Germany (https://www.uponor.com) for precise loop-by-loop temperature control. Position B houses the Uponor Smatrix Base PRO Controller X-147 Bus together with the Smatrix PULSE Com R-208 communication module and the Uponor Smatrix Base PULSE controller, enabling wireless coordination across all zones. At position C, the wall-mounted Uponor Smatrix Base digital thermostat integrates relative-humidity and operative-temperature sensing to fine-tune setpoints. This configuration delivers accurate, energy-efficient management of the underfloor heating system.

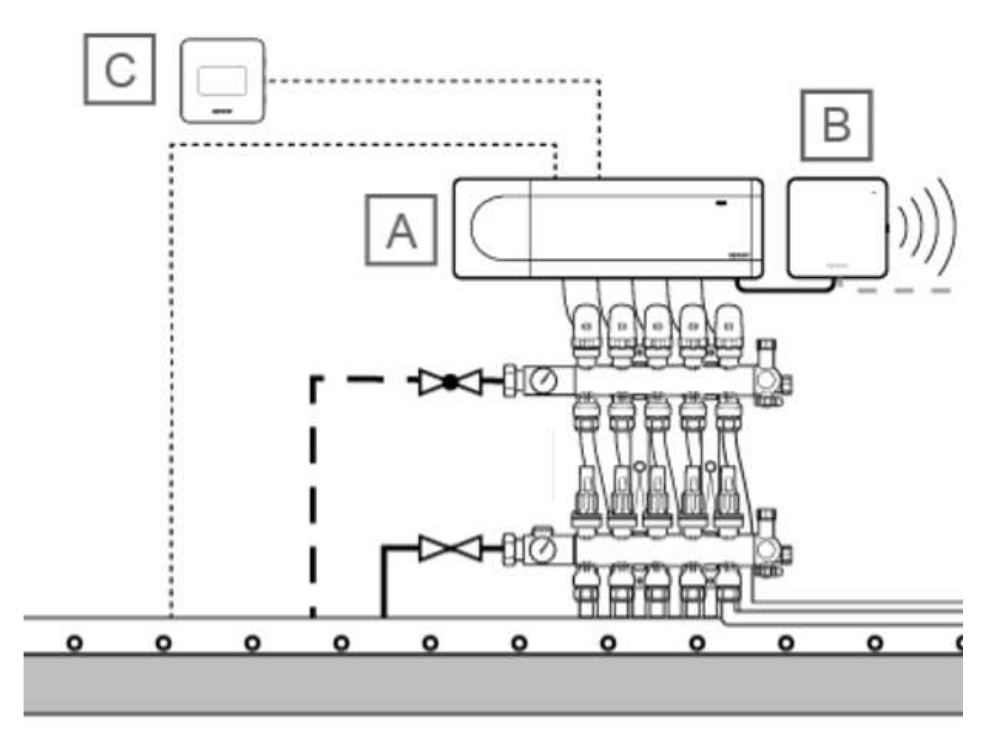


Figure 3:Underfloor heating manifold with vario actuators and Uponor smatrix controls [Credits: Uponor]

2.2. MANIFOLD PERFORMANCE ASSESSMENT

This section provides a comprehensive analysis of the preliminary low-temperature heating design, assessing circuit surface temperature uniformity, evaluating heat-output distribution, quantifying circuit pressure drops, and reviewing supply, return and ΔT profiles for each loop.

2.2.1. CIRCUIT SURFACE TEMPERATURE ANALYSIS

Figure 4 plots every circuit surface temperature across Manifolds M1-M7. Each star marks a surface temperature per circuit. The dashdot line shows the mean for that manifold, while the dashed lines mark ± 0.5 °C bounds. All 127 circuits across Manifolds M1-M7 with an overall mean of 24.53 °C and a standard deviation of only 0.29 °C. Fully 96.7% of circuits fall within ± 0.5 °C of their manifold's mean.

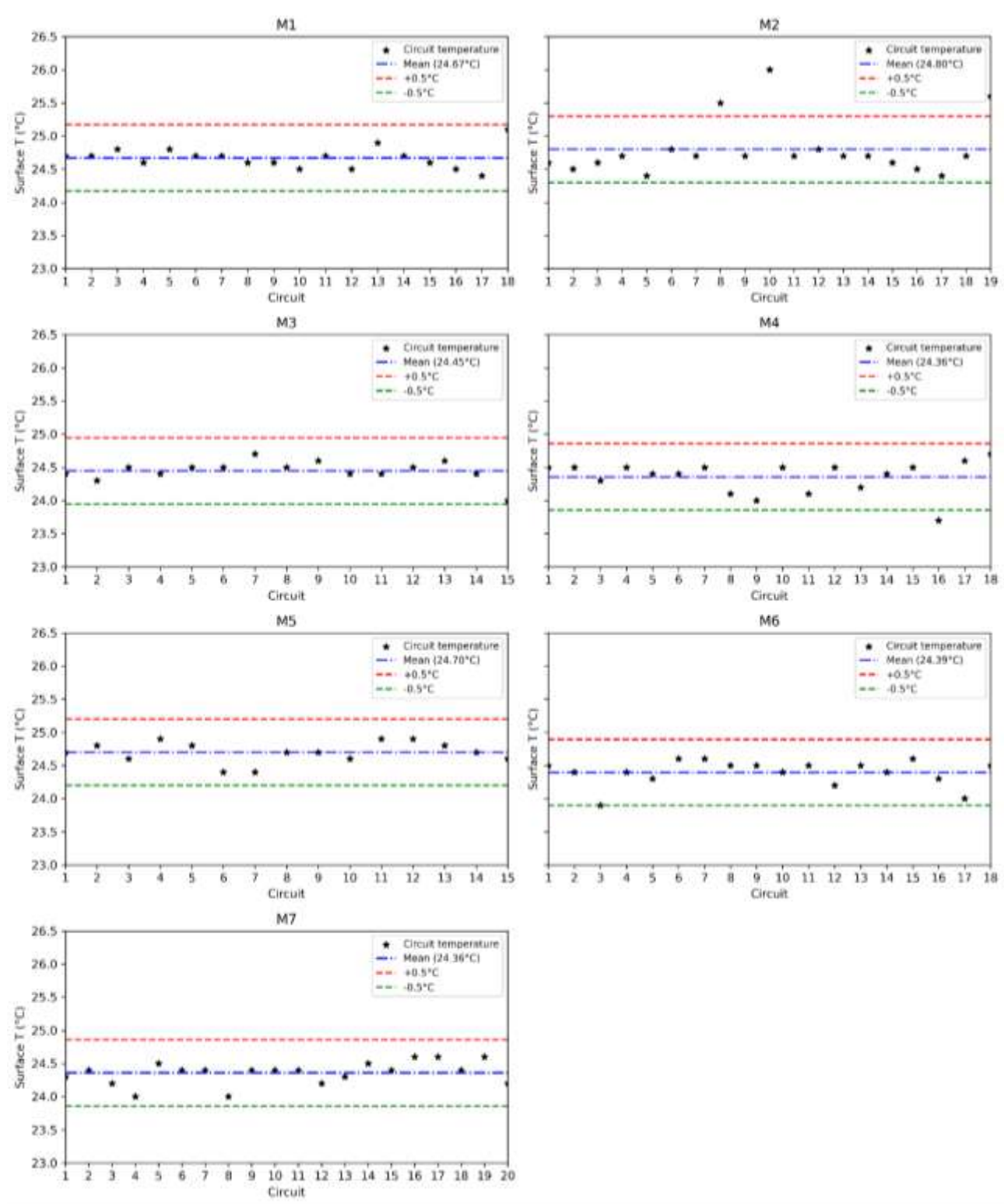


Figure 4: Surface Temperature per circuit by manifold (M1–M7)

2.2.2. HEAT OUTPUT DISTRIBUTION ANALYSIS

The violin plots in Figure 5 show how individual circuits deliver heat output across manifolds M1-M7. Each red "violin" traces the density of circuit outputs, the black stars mark each loop heat output, and the diamond symbol indicates the mean per manifold. Overall, circuit outputs span roughly 600 W up to 3200 W. Manifold M5 has the highest average at about 1500 W and the widest spread reflecting its mix of long loops in large zones while M4 sits lowest around 1100 W with a tighter distribution, consistent with its shorter, more uniform circuits. Despite these differences, every manifold meets its targeted heating demand without extreme outliers. The density curves show most circuits cluster within ±300 W of their mean.

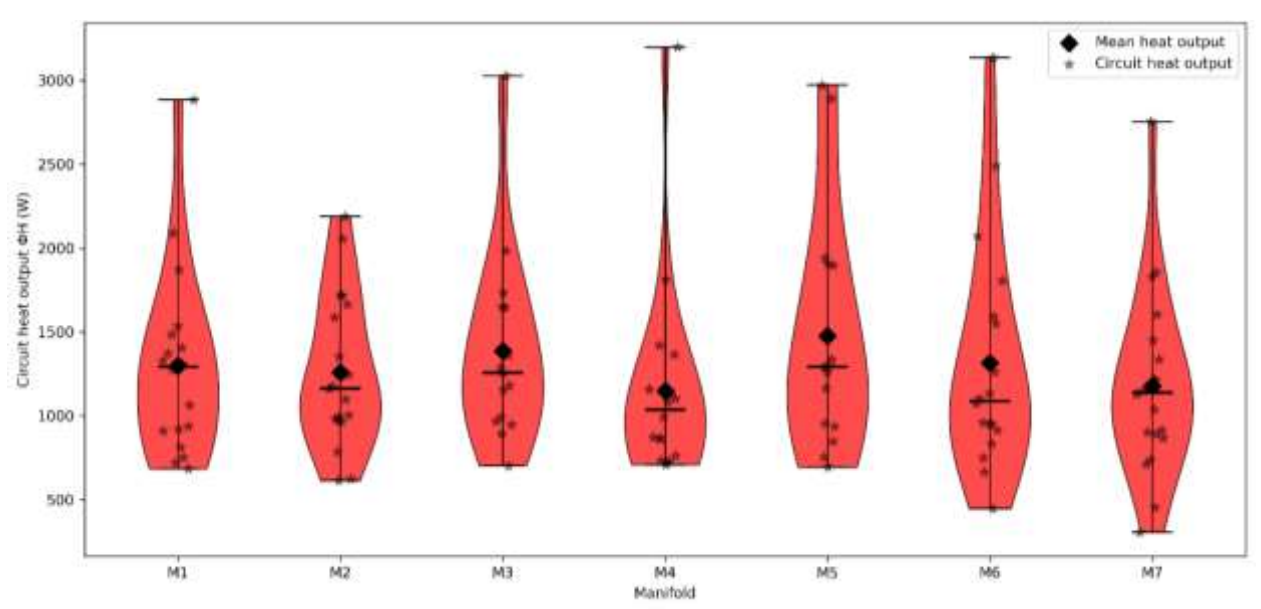


Figure 5: Heat output distribution per circuit by manifold

2.2.3. CIRCUIT PRESSURE DROP ANALYSIS

Figure 6 plots show the total pressure loss Δp for every Comfort Pipe PLUS circuit across manifolds M1-M7. Loop lengths span 67.7 m (M6-Circuit 2) to 129.7 m (M5-Circuit 7), and Δp values range from 28.6 kPa to 64.3 kPa. Manifold M5 exhibits the highest mean pressure drop, 58.0 kPa, driven by its longer average loop length (\approx 108 m) and peak Δp of 64.3 kPa on the 129.7 m circuit. In contrast, M6 (mean length \approx 75 m) and M4 (\approx 80 m) record the lowest mean Δp 32.1 kPa and 33.7 kPa respectively with minimum drops of 28.6 kPa and 29.2 kPa on their shortest loops.

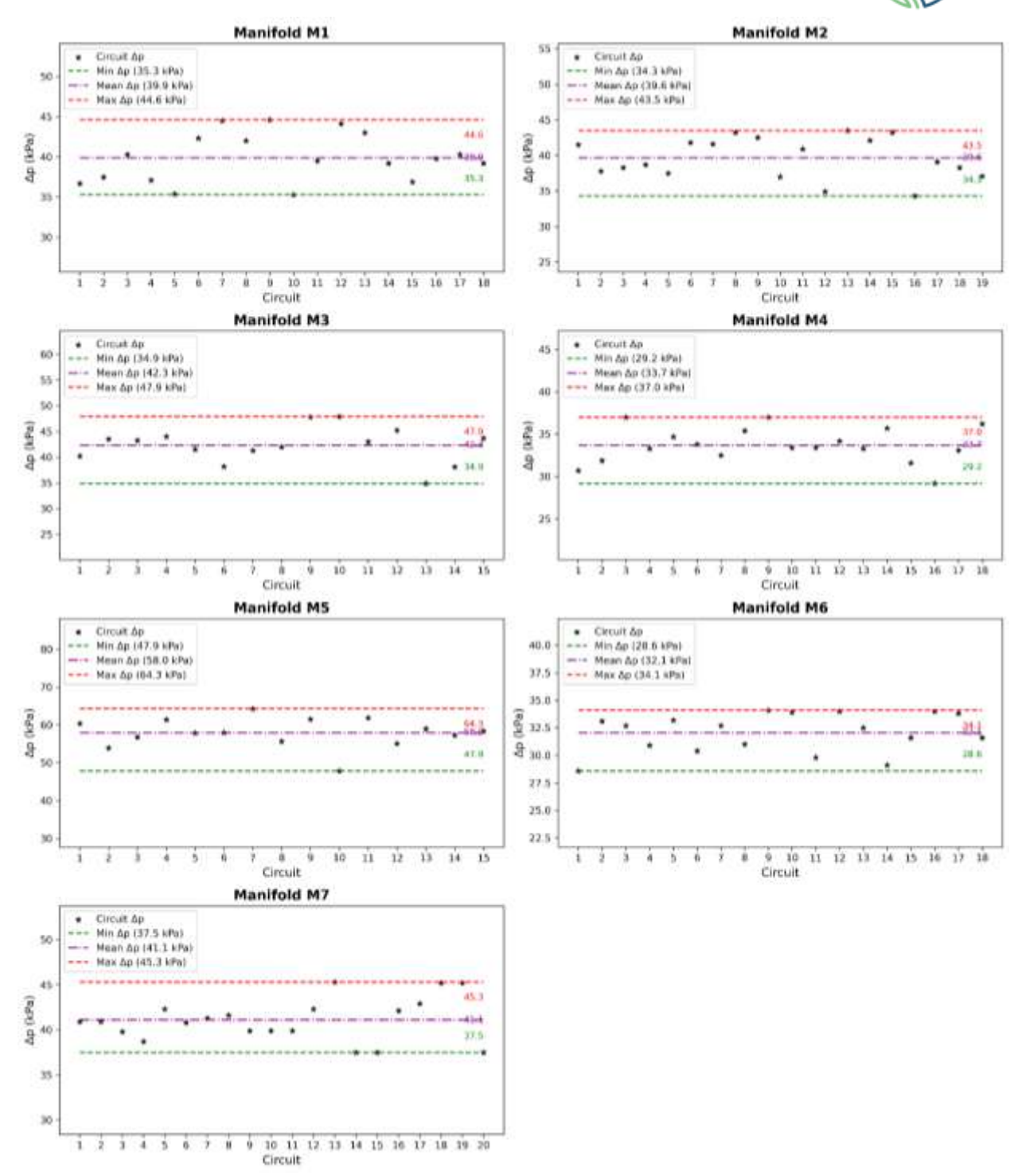


Figure 6:Total pressure loss Δp per circuit by manifold

2.2.4. SUPPLY, RETURN AND ΔT PROFILES PER CIRCUIT

Figure 7 shows the estimated supply temperature in red from the return temperature from district heating through the low temperature substations, the return temperatures (blue) and the resulting ΔT (green) for every circuit across Manifolds M1-M7. Overall circuit lengths vary from a minimum of 67.7 m (M7-Circuit 12) to a maximum of 129.7 m (M5-Circuit 6). Corresponding ΔT values span from 5.0 K on the shortest circuits (e.g., M7-C12 at 67.7 m) up to 6.2 K on the longest loop (M5-C6 at 129.7 m).

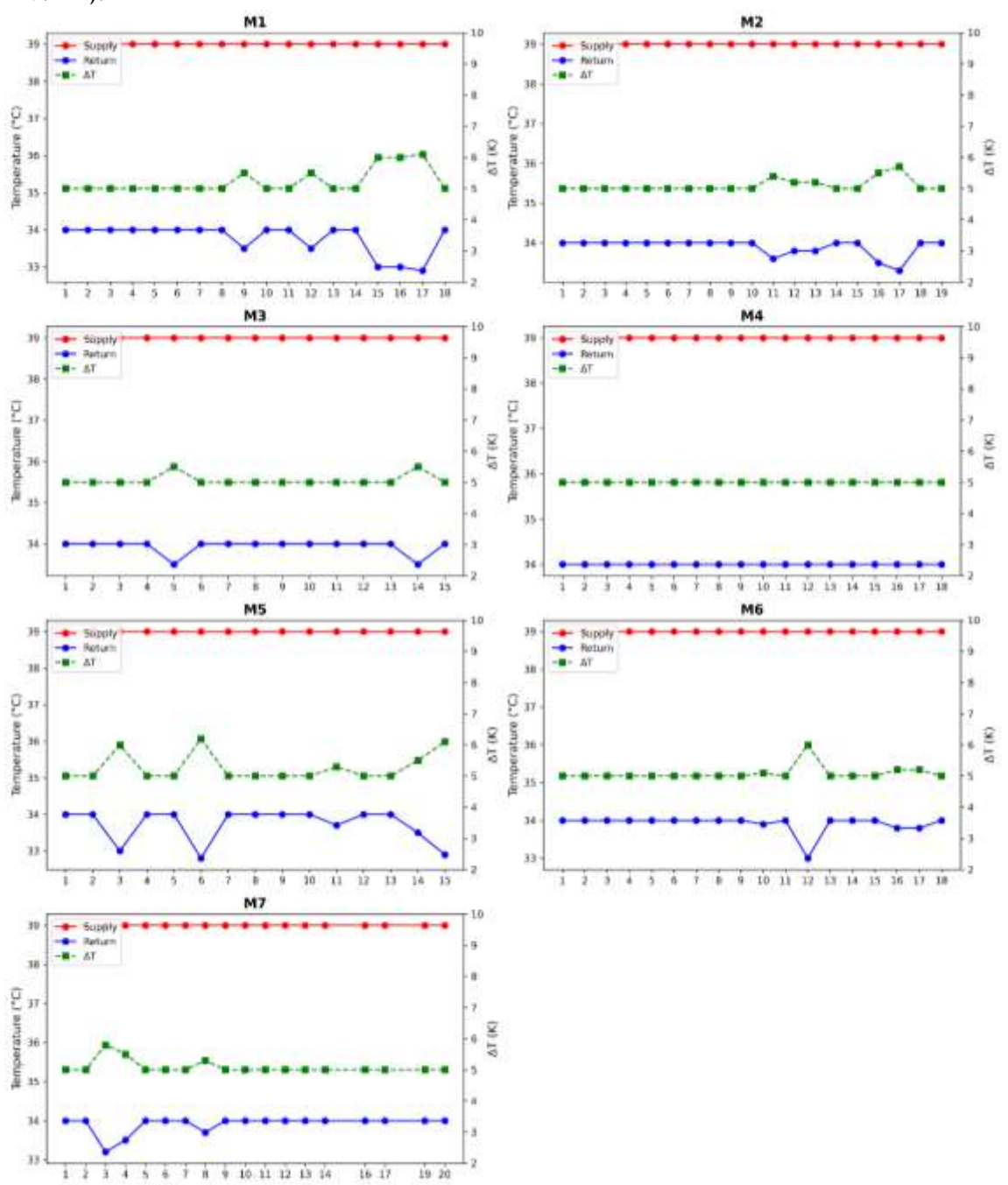


Figure 7: Supply/return temperature and ΔT per circuit by manifold

3. RENEWABLE ENERGY-BASED HVAC SOLUTION DEVELOPMENT FOR THE DEMONSTRATION SITE OF RIGA MARKET

3.1. BACKGROUND AND CONTEXT

The building sector contributes approximately 40% of global greenhouse-gas emissions when both embodied and operational carbon are accounted for (European Union 2024). Yet annual renovation rates remain low just 1% of the existing stock and only 5% of new buildings achieve net-zero performance (Falana et al 2024). Meanwhile, global building floor area is projected to nearly double by 2050. Without rapid scale-up of renovation and deployment of low-carbon HVAC technologies, sector emissions will continue to rise. Low-temperature heating (LTH) and high-temperature cooling (HTC) represent a promising solution. These water-based systems integrate directly into floors, operating with modest temperature lifts that enhance building thermal inertia (Zhao C et al 2023). The added thermal mass smooths indoor temperatures during transients, increases resilience to short-term supply disruptions and extreme weather, and aligns with renewable and low-exergy sources such as solar thermal, geothermal, low-temperature district heating and heat pumps (Quirosa et al. 2022). Moreover, LTH and HTC have therefore potential for increasing the efficiency of heat pumps, as the smaller temperature differential reduces the work requirement of heat pump compressors, boosting overall efficiency (Liu X et al 2017).

3.2. RIGA MARKET DESCRIPTION

The Riga Central Market pavilion (Figure 8) serves as the Latvian MULTICLIMACT demonstration site, existing building (top) and IFC model (bottom). The pavilion building height is 21 m with 70.45 m (length) by 35.26 m (width), and the building volume is 53,408 m³.





Figure 8: The selected pilot for LTH in MULTILCIMACT - existing building (top) and IFC model (bottom) [Credits: Riga Municipality]

The energy audit and preprocessing carried out by the Riga team revealed that the pilot pavilion is a district-heated, heritage-listed structure served by the central DH network. Figure 9 presents the existing substation layout at Riga Central Market pavilion, showing five plate-type heat exchangers tied into the primary loop. These comprise a 1800 kW unit for domestic hot water, a 300 kW heating exchanger and three ventilation-air exchangers rated at 428 kW (serving two pavilions), 540 kW and 311 kW. Color-coded piping delineates each loop, and annotated labels indicate each exchanger nominal capacity.

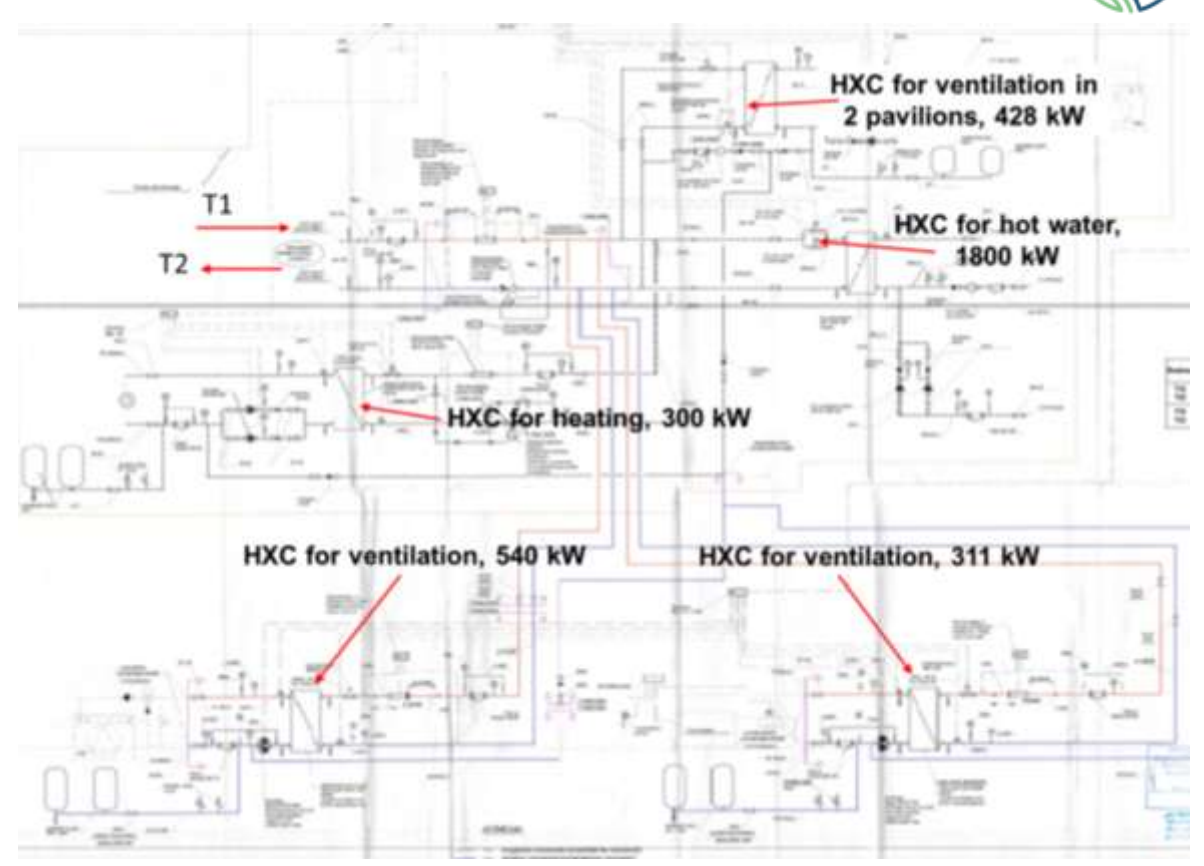


Figure 9:Heating unit conceptual diagram [Credits: Riga municipality]

Figure 10 illustrates the Temperature regime in DH network (Second generation district heating "2nd GDH"). The plot shows two curves: the supply temperature (T_1), and the return temperature (T_2). Both temperatures are modulated in response to the outdoor air temperature, following Latvian Building Standard LBN 003-19 guidelines. Under extreme design conditions (-20 °C outdoor), the network ramps up to a 120 °C supply and 70 °C return. As outdoor temperatures rise toward the seasonal average of 1.1 °C, T_1 gradually decreased into 64-68 °C while T_2 stabilizes around 42-46 °C.

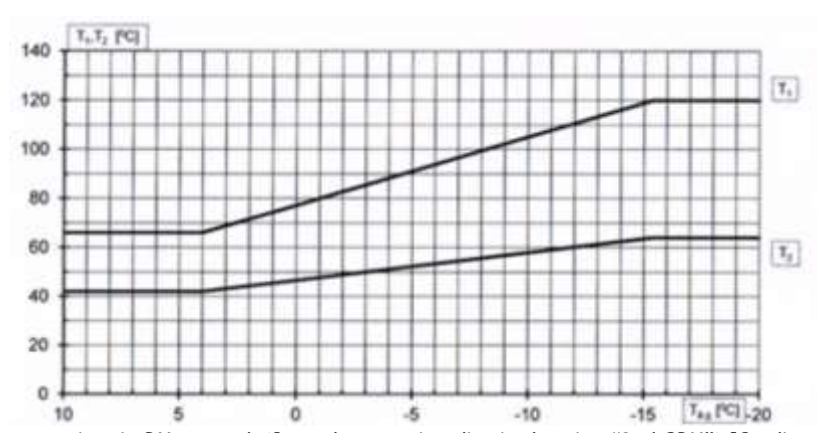


Figure 10: Temperature regime in DH network (Second generation district heating "2nd GDH") [Credits: Riga municipality]

Riga's district heating network serves roughly 70% of the city residents, delivering over 3100 GWh of thermal energy to the network in 2023. The system relies on a combination of combined heat and power (CHP) plants and dedicated boilers. Natural gas and wood chips are the primary fuels, with biomass playing an increasingly prominent role: in 2023, 41.3% of the heat supplied came from wood-chip sources (12.9% from biomass CHP and 28.4% from biomass boilers), in full compliance with the EU Renewable Energy Directive (2018/2001).

3.2.1. BUILDING THERMAL BALANCE

Figure 11 (top) illustrates the monthly heating balance of the pavilion based on the auditing data supplied by Riga pilot, expressed per square meter of floor area. The grey bars show the specific heating demand, while the yellow bars represent monthly internal and solar gains that offset those losses. In winter (January-March and November-December), heat losses far exceed gains, requiring net heat supply of up to 20-30 kWh/m²-month. In contrast, Figure 11 (bottom) presents the pavilion cooling balance over the same annual cycle. The blue bars denote the specific useful cooling demand that is, the net cooling load after accounting for internal heat gains (yellow line) and envelope losses (light-blue shading). Cooling demand is negligible from September through May, then spikes in July (\approx 12 kWh/m²-month) and August (\approx 8 kWh/m²-month) as internal gains peak and envelope losses remain significant. The grey shading behind the blue bars shows the total heat that must be evacuated (i.e. the sum of envelope gains and internal gains), which in midsummer reaches nearly 70 kWh/m²-month.

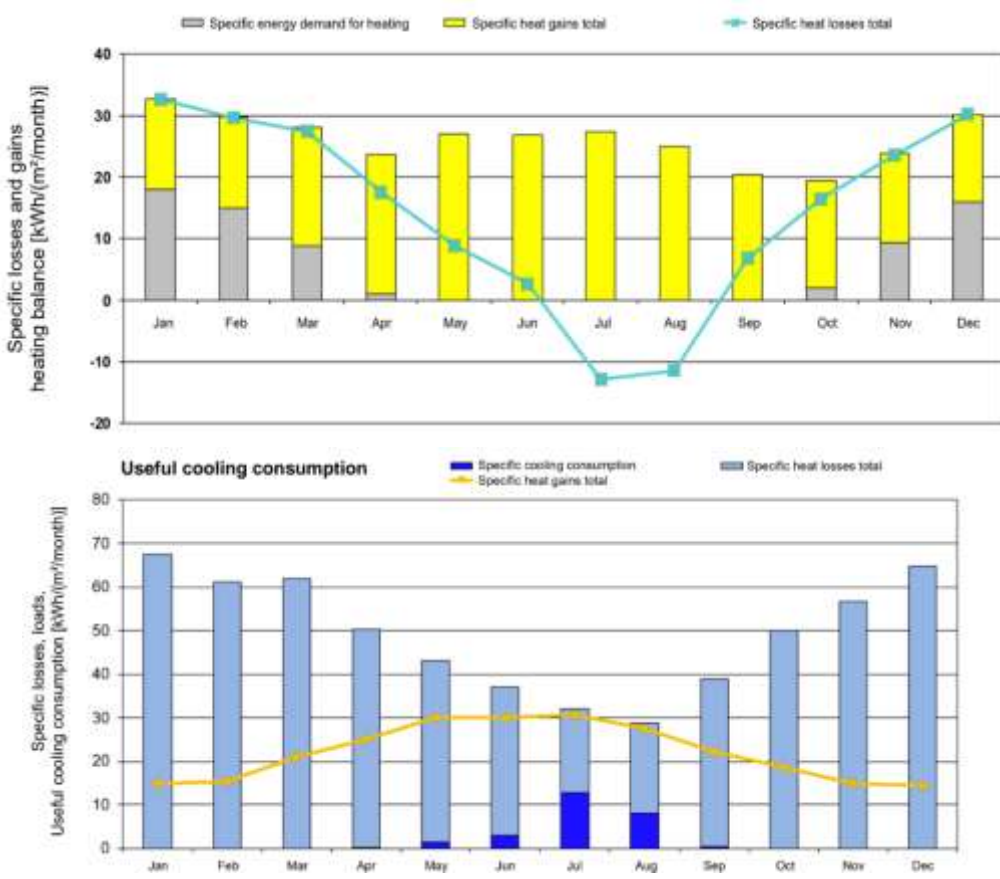


Figure 11: Monthly heating and cooling energy balance [Credits: Riga municipality]

3.3. PROPOSED RENEWABLE-ENERGY-BASED HVAC CONCEPT

In this Task, the main work has been carried out by KTH and Uponor is to propose a future climate resilience scenario for renewable energy-based HVAC system built around five key components: a building-integrated photovoltaic (BIPV) system, a reversible heat pump (HP), the district heating network low-temperature substation, and a combined low-temperature (DH), a heating/high-temperature cooling (LTH/HTC) distribution network consisting of seven manifolds and their associated underfloor circuits as shown in Figure 12. In heating mode, return water from the DH network (typically 42-46 °C) feeds the low-temperature substation, where it is tempered and then distributed to the seven manifolds. From each manifold, water circulates through the radiant floor heating loops to meet the building's thermal demand. The heat pump acts as a backup source, boosting supply temperature if necessary. In cooling mode, the heat pump operates in reverse to chill water down to around 16-18 °C and supply the HTC network. The chilled water is distributed through the same manifolds and underfloor circuits, now serving as radiant cooling emitters. Meanwhile, the BIPV system provides on-site electricity for the heat pump, with any surplus exported to meet the pavilion general electrical loads.

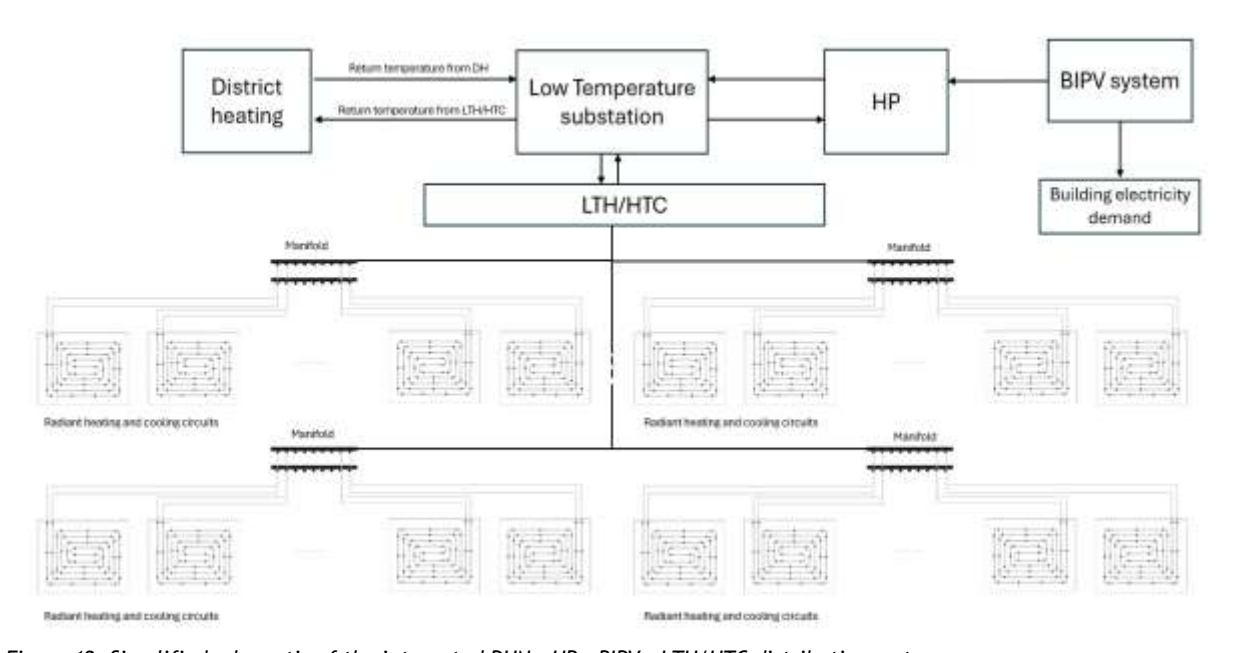


Figure 12: Simplified schematic of the integrated DHN - HP - BIPV - LTH/HTC distribution system

The designed 65 kWp BIPV system on the Riga Central Market pilot delivers a highly seasonal energy profile, with outputs ranging from just over 1000 kWh in the darkest winter months to nearly 9600 kWh in May (Figure 13). During December and January, when daylight hours and solar angles are lowest, the system produces roughly 850-1037 kWh per month. As spring arrives, generation increases surpassing 4500 kWh in March, 7069 kWh in April, and peaking at 9538 kWh in May. Summer yields remain robust, with July delivering 9294 kWh and June 8752 kWh, before tapering off through autumn to 2740 kWh in October. Over the course of a full year, this BIPV installation is expected to generate approximately 65000 kWh of clean electricity, directly offsetting roughly 48 kW of heat pump electrical demand and with any surplus exported to meet the pavilion general electrical loads.

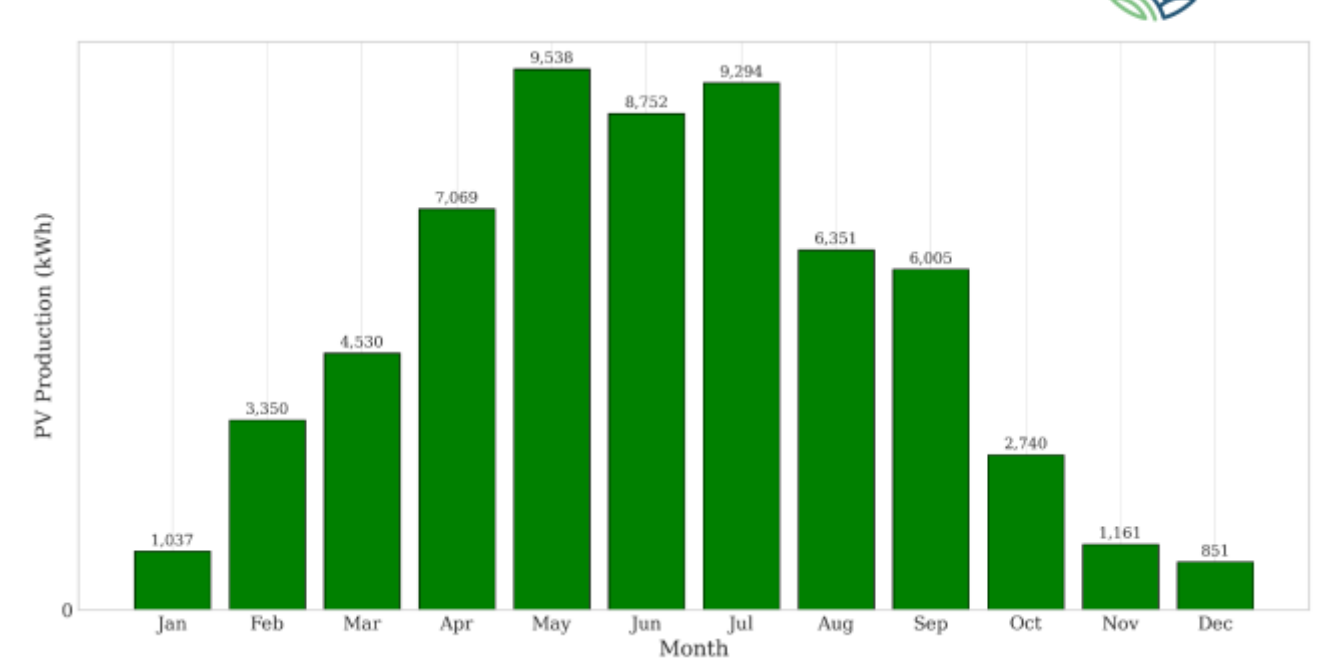


Figure 13: Monthly PV production - 65 kWp BIPV system

Figure 14 compares the Uponor designed (blue circles and lines) versus simulated (orange squares and dashed lines) heat outputs for each circuit across the seven UFH manifolds (M1-M7). The mean absolute percentage error (MAPE) was used as it normalizes the average absolute error, enabling direct comparison of relative deviations across circuits with varying heat outputs. The tight overlap between the curves—and low permanifold MAPE values from 1.5 % to 3.9 % confirms that the calibrated model reproduces UPONOR's design targets with high accuracy. For instance, Manifold M3 archives a MAPE of only 1.5 %, indicating sub50 W deviations in most of its ten circuits—well within typical design tolerances. Even the "worst" manifold, M2, maintains a MAPE under 4 %, demonstrating the model reliability across a wide range of circuit lengths, flow rates, and floor areas. These validation results build confidence that the UFH simulation will predict indoor temperature responses under varying schedules and weather conditions. With each circuit thermal behavior reliably captured, the model provides a solid foundation for the forthcoming comfort and resilience analyses.

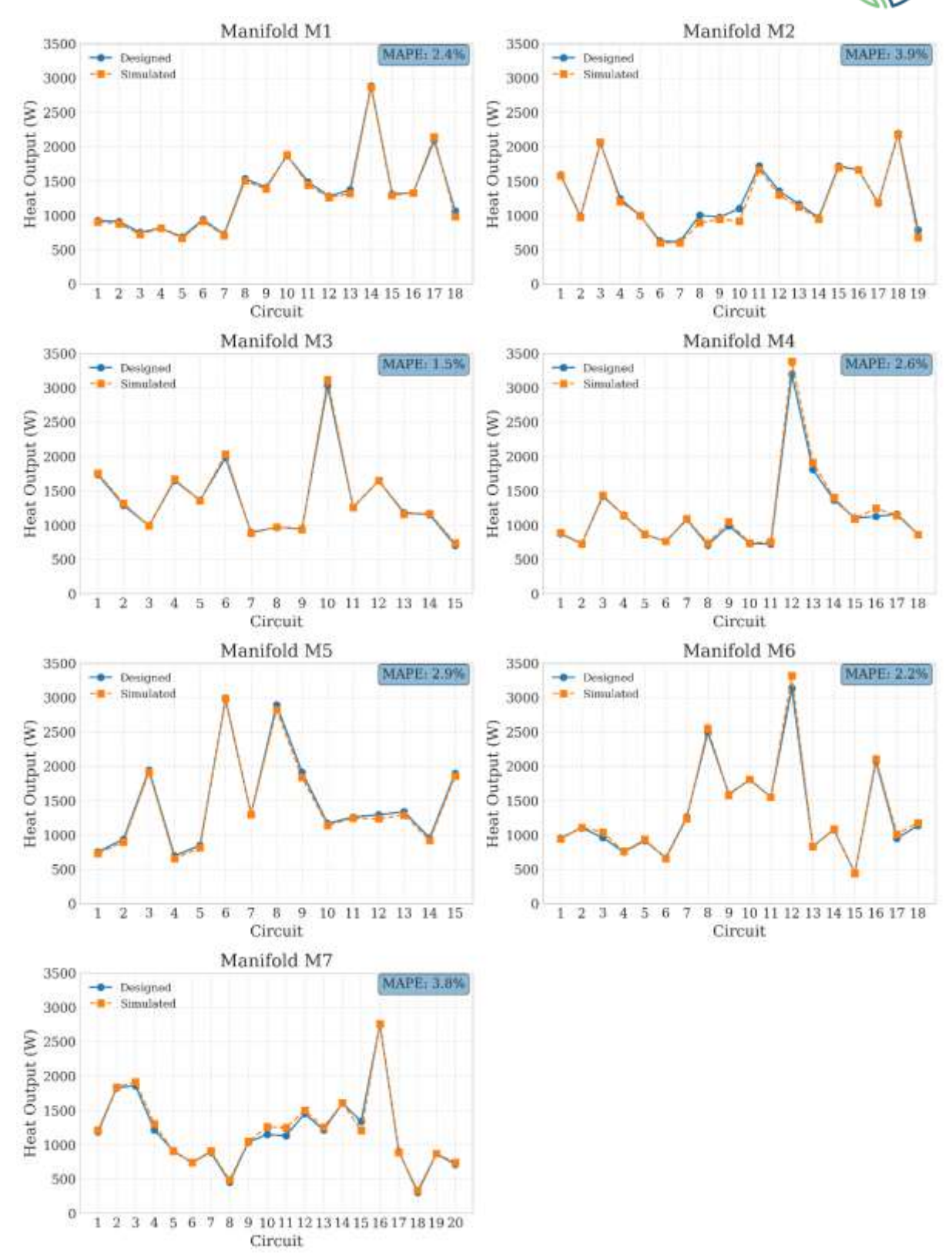


Figure 14: Comparison of designed vs. simulated heat output per circuit across UFH manifolds

3.4. RESILIENCE ASSESSMENT

In this Task, the resilience of the LTH/HTC system is assessed by testing its ability to maintain acceptable indoor conditions under two complementary stress-test scenarios—a cold wave and a heat wave—using a validated model.

3.4.1. COLD-WAVE SCENARIO ANALYSIS

To evaluate winter resilience, a uniform -10 $^{\circ}$ C shift was imposed on a two-week January weather record for Riga, creating an extreme cold-spell profile. Under this "cold-wave" forcing, outdoor temperatures drop by ten degrees. The base control strategy runs underfloor heating from 07:30 to 18:00 h; outside those hours, the system remains off. Five variants were simulated to explore proactive strategies, in which the UFH system start 1, 2, 3, 4, or 5 hours earlier than 07:30 h ("preheat offsets"). Indoor comfort is evaluated against a ± 2 $^{\circ}$ C band around a 16 $^{\circ}$ C setpoint. The 16 $^{\circ}$ C setpoint was selected by the REA team by comparing indoor temperature trajectories and comfort-deviation metrics across offsets, quantifying how much earlier preheating improves resilience during severe cold.

Figure 15 illustrates indoor temperature (orange) under a coldwave event (blue dashed) for five preheatoffset strategies. Each subplot shows the comfort band (±2 °C around 16 °C), the standard heating window (07:30-18:00 h, shaded orange), and the preheat period (shaded red) beginning 1-5 hours before 07:30 h. With only a 1 h preheat, indoor temperatures frequently dip below 16 °C, especially during the first hours of each day, resulting in comfort violations 42.9 % of the time. As the preheat window lengthens, the indoor curve shifts upward: a 3 h offset keeps temperatures within the comfort band nearly 78 % of the time, and a 5 h offset further improves that to 83.1 %. Notably, none of the strategies overshoot above 20 °C, demonstrating that extended preheating does not cause overheating under this control logic. These results are supported by the building thermal inertia—calculated at approximately 8.2 hours which acts as a buffer against rapid temperature swings. The embedded underfloor heating network further enhances this inertia: by precharging the slab with heat, it stores energy and slowly releases it throughout the day.

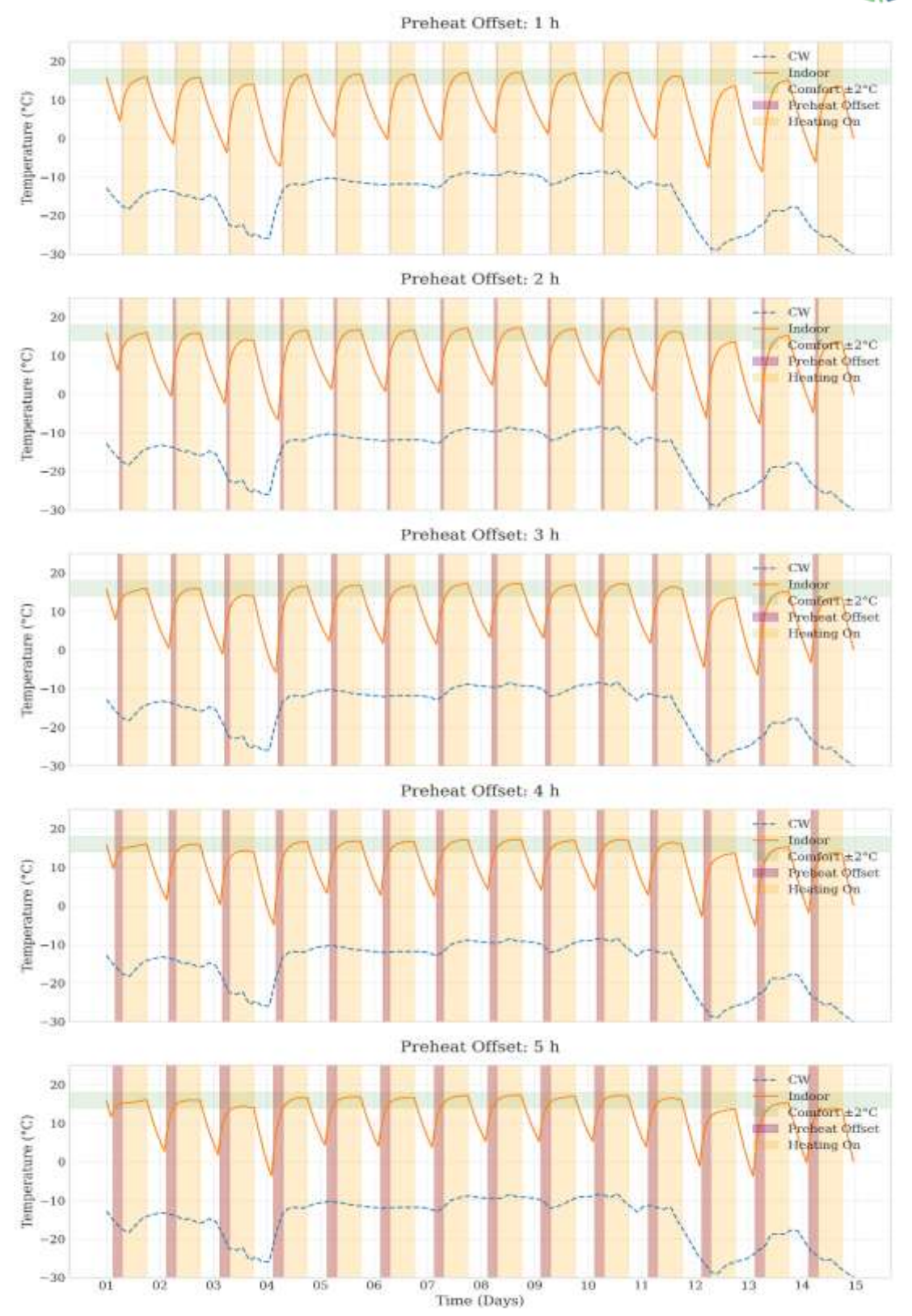


Figure 15: Indoor and outdoor temperature profiles during cold-wave scenario with preheat offsets (1–5 h)

3.4.2. HEAT-WAVE SCENARIO ANALYSIS

Conversely, the "heat-wave" scenario tests summer resilience by uniformly adding ± 10 °C to a mid-July two-week temperature series, representing an extreme heat event. The chilled-slab cooling system is scheduled to operate from 07:30 to 18:00 h, with no cooling at night. As with the cold-wave case, five "pre-cool" offsets were introduced of 1-5 hours before 07:30 h to assess whether starting the cooling loops earlier lowers peak indoor temperatures and reduces comfort deviation. Comfort is defined by a ± 2 °C band around a 26 °C cooling setpoint. The 26 °C setpoint was selected by the REA team. The performance of each offset is then evaluated using the same suite of deviation metrics, revealing how pre-cooling strategies and the building thermal inertia jointly sustain comfort under extreme heat.

Figure 16 presents the outdoor heatwave profile (dashed blue) and indoor temperatures (solid orange) under each precool offset. The light green band marks the comfort range (24-28 $^{\circ}$ C), blue shading shows active cooling periods, and purple bars indicate the precool windows. With only a 1 h precool, indoor temperatures exceed 28 $^{\circ}$ C nearly 39 $^{\circ}$ 6 of the time, while undercooling below 24 $^{\circ}$ C occurs in only 1.8 $^{\circ}$ 6 of hours. Extending the precool horizon reduces overheating by roughly three percentage points per additional hour: a 3 h offset lowers exceedance to 32.7 $^{\circ}$ 6, and a 5 h offset further cuts it to 26.8 $^{\circ}$ 8. Although undercooling rises to 7.1 $^{\circ}$ 8 with a 5 h offset, indoor temperatures never fall below 23 $^{\circ}$ C7, which is extra comfortable. The building thermal inertia ($^{\circ}$ 8.2 h), as the precool charge stored in the slab, early activation of the chilled-slab network leverages this inertia, smoothing indoor temperatures and enhancing occupant comfort under extreme heat events.

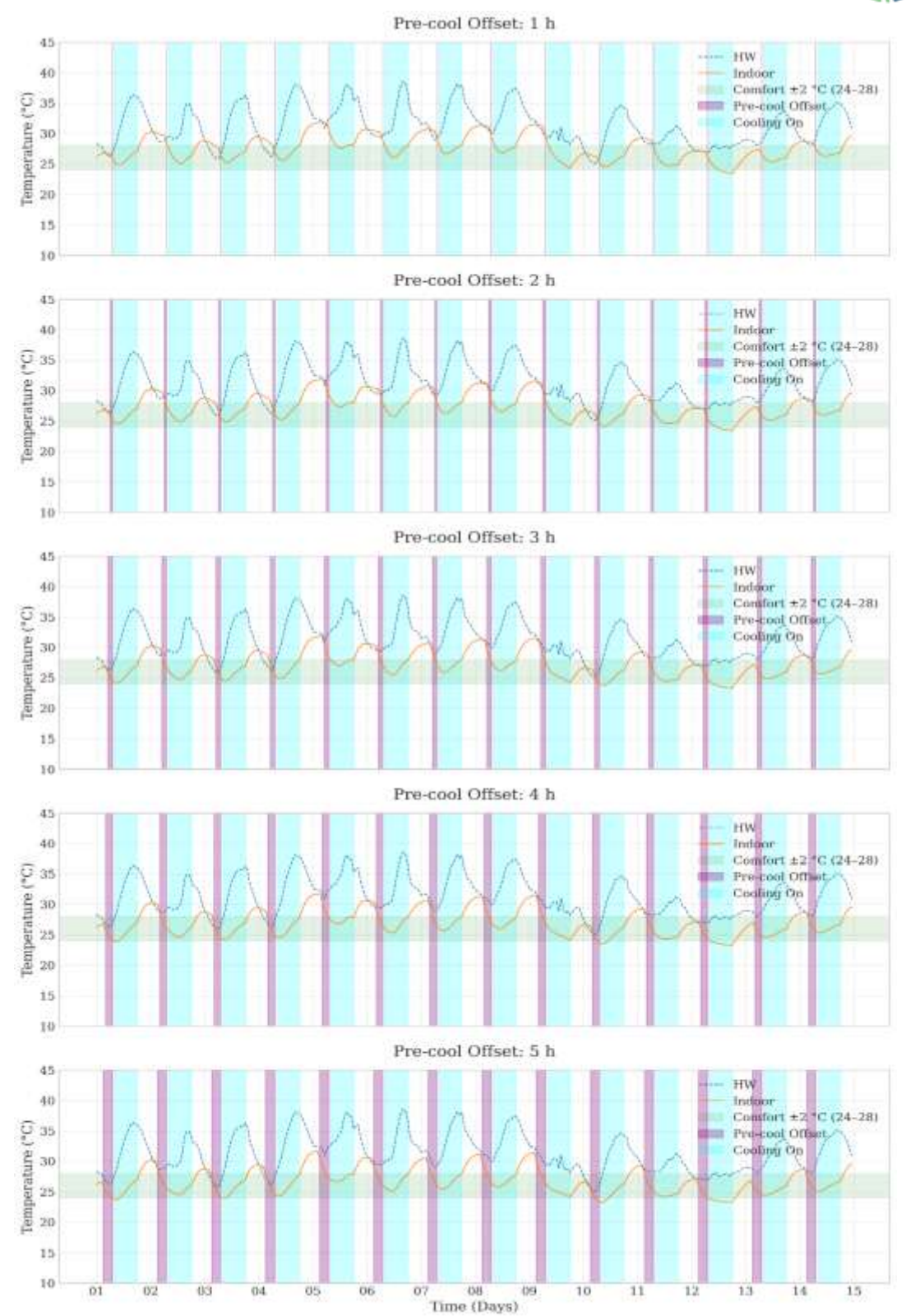


Figure 16: Indoor and outdoor temperature profiles during heat-wave scenario with precool offsets (1–5 h)

4. DEVELOPMENT OF SENSORIZED CEMENTITIOUS BLOCKS FOR STRUCTURAL HEALTH MONITORING PURPOSES

Regularly monitoring a building or an infrastructure is pivotal to maximize its life cycle and timely intervene if needed. Different techniques can be exploited to this aim, like self-sensing/monitoring techniques (Mobili et al.), smart sensor networks exploiting deep learning computing tools (Sofi et al.), acoustic sensors (Ozelim et al.), piezoelectric transducers (Gayakwad and Thiyagarajan), noncontact vibration sensors (Klun et al.), accelerometers (Li et al.), etc. In last decades, a lot of research has been performed on the development of sustainable self-sensing materials coupled with related measurement system, capable to provide an insight into multiple aspect of structural health: not only the presence of external loads, but also variations in thermos-hygrometric conditions and penetration of contaminants, just to cite a few examples. Structural Health Monitoring (SHM) is pivotal to promptly define the onset of deterioration phenomena allowing to act immediately on a structure when the investigated parameters deviate from the "normal" trend. This means that something in the external or internal characteristic of the material has changed, which could represent a possible damage. SHM methods based on self-sensing concrete are particularly advantageous in terms of sensitivity, durability, ease of installation and maintenance (Wen and Chung) and are implemented generally through measurements of the concrete electrical properties such as electrical resistance, impedance or resistivity (Cosoli et al.). Generally, carbon-based materials are added to cementitious materials to enhance their electrical properties; however, pure and highly expensive commercial materials are used. In this context, UNIVPM developed and patented a novel environmentally friendly cement-based material with reduced electrical impedance for SHM purposes (patent n. 102020000022024). During the first 12 months of the MULTICLIMACT project (first reporting period), the UNIVPM mortar was studied in terms of self-sensing and vibrational properties. The results were reported in "D3.3 - Review, design and specifications of cutting edge, evolutive, self-sensing and multifunctional materials and technologies for improving the resilience of buildings, including cultural heritage". During the following 12 months of the MULTICLIMACT project (second reporting period), the UNIVPM self-sensing mortar was used to cast sensorized mortar blocks to be connected to the LIS' monitoring platform; preliminary monitoring tests have been executed in LIS offices in close collaboration between UNIVPM and LIS.

4.1. CASTING OF SENSORIZED BLOCKS

Within the framework of T3.3, UNIVPM planned the installation of the monitoring solution in the Italian pilot. Sensorized mortar blocks were designed and two different types of sensors were selected:

- Electrical impedance sensors: n. 4 stainless-steel electrodes were embedded in the specimens, maintained in position through a 3D-printed TPU array. For signal acquisition, a low-cost board was selected (i.e., EVAL-AD5940BIOZ, based on the AD5940 chip, by Analog Devices, Wilmington, Massachusetts, US, https://www.analog.com/).
- Free corrosion potential sensors: a commercial pseudo-reference electrode (Cescor S.r.l., Milan, Italy, https://www.cescor.it/), realized in titanium activated with mixed metal oxides enriched with iridium (TiMMO), was anchored to a steel rebar inside the specimen to measure the free corrosion potential of the steel reinforcement.

Two of these blocks, with dimensions $100 \times 100 \times 230$ mm, were produced following a mix design defined from a UNIVPM patent (n. 102020000022024, filed on 18/09/2020) regarding an innovative, sustainable, self-sensing cementitious conglomerate based on low cost carbon-based additions, namely biochar (BCH) and recycled carbon fibres (RCF). Indeed, these blocks have a stainless steel reinforcement inside, which was used also for the sensors' installation.

4.1.1. CASTING PROCEDURE

At first, the moulds to cast the blocks were prepared; in particular, ad-hoc wooden panels (2.7 cm-thick) were cut and assembled to this scope (Figure 17).



Figure 17 Drawing of the wooden panels used to realize the moulds. Dimensions are reported in mm (picture courtesy of UNIVPM).

The wooden panels were assembled through self-tapping screws with a diameter of 3.5 mm and a length equal to 50 mm (Figure 18).

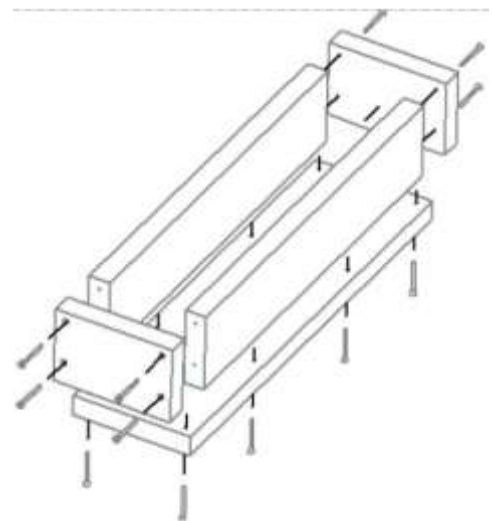


Figure 18 Scheme of the wooden mould assembly (picture courtesy of UNIVPM).

Then, holes in the shorter lateral panels were realized to create the passage for PVC tubes (DN 32) necessary to host the sensors cables as well as the reinforcements. Corrugated carbon steel rebars had a length of 35 cm and a diameter of 8 mm; a rebar was positioned inside each wooden mould and the sensors were anchored to it through plastic ties. For the following free corrosion potential measurements, a preparatory activity was performed on the rebars as follows:

- At first, acetone was used to degrease rebar extremities
- The rebar surface was cleaned through a metallic brush to remove corroded areas

- The ground extremity was treated with lubricant oil to avoid overheating phenomena and a hole realized through a drill press with a 3 mm-tip
- Another grinding was performed to remove possible deburring
- The steel wire (0.75 cm-diameter) was passed through the hole, making a knot in the form of a noose and attaching it to the rebar through soldering (Figure 19).
- A rebar extremity was ground to realize a hole through which a steel wire was hook
- subsequently the wire was covered by silicon and stripped for few cm to allow the measurement of the rebar potential.

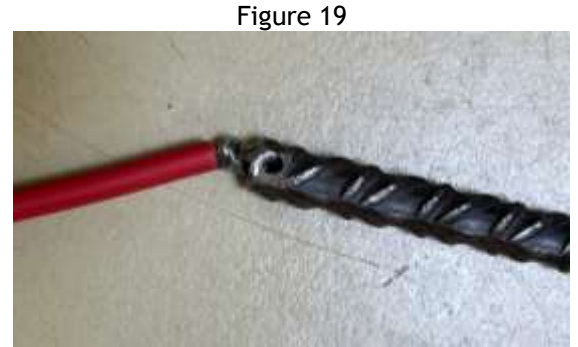


Figure 19 Connection between rebar and wire for the free corrosion potential measurement (picture courtesy of UNIVPM).

To protect the junction as well as the rebar extremities, a two-component epoxy (1:5 ratio) was employed paying attention to avoid uncovered areas (Figure 20).



Figure 20 Protection of rebar extremities through the application of a two-component resin (picture courtesy of UNIVPM).

Concerning the measurement of electrical impedance, as done in previous tests performed within the project (see for example D3.3 "Review, design and specifications of cutting edge, evolutive, self-sensing and multifunctional materials and technologies for improving the resilience of buildings, including cultural heritage"), the Wenner's method (Wenner) was exploited, using 4 electrodes in alternating current to avoid the polarization of both material itself and at the interface between electrodes and material (Cosoli et al.). The electrodes were realized employing stainless steel screws, around which electrical wires were wrapped (Figure 21); hence, the electrodes were hosted (equidistant) in a 3D-printed case (in TPU, thermoplastic polyurethane).

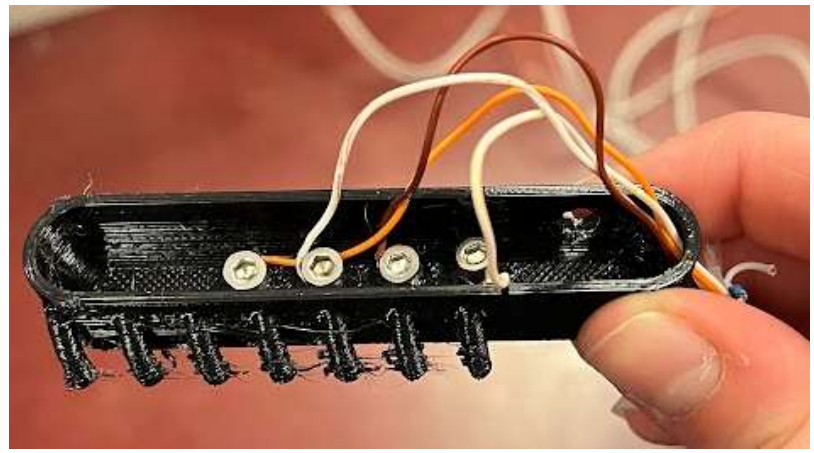


Figure 21 Electrodes within the 3D-printed case and related cables (picture courtesy of UNIVPM).

At the end, the whole system was protected filling the TPU case with silicon; on the other extremities of the electric wires, dedicated pins were soldered to ease the connection with the acquisition system (i.e., acquisition board EVAL-AD5940BIOZ, based on the AD5940 chip, by Analog Devices). Hence, the board must be connected to a PC. Data can be acquired through the SensorPal software (Analog Devices); in particular, the modulus and the phase of the electrical impedance are recorded at a certain measurement frequency (i.e., 10 kHz in this study). The connection setup is reported in Figure 22; electric current is injected through working electrode and counter electrode (WE and CE, respectively), then the corresponding voltage is measured between sensing and reference electrodes (SE and RE, respectively).

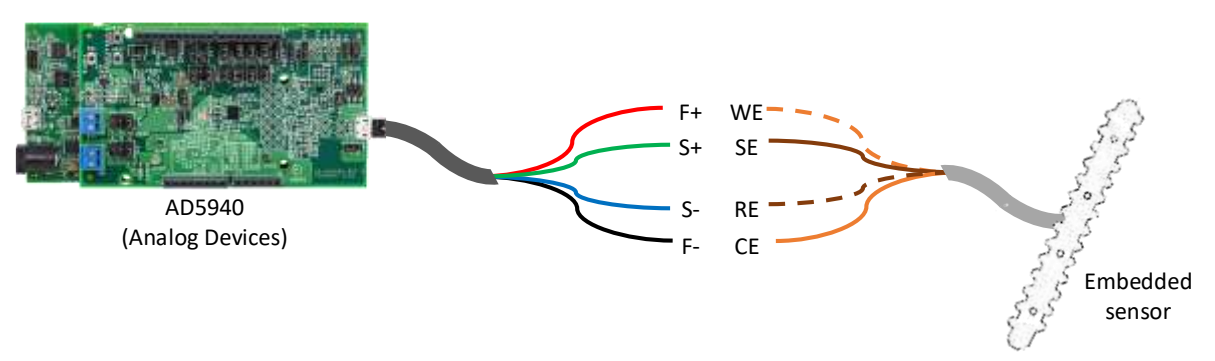


Figure 22 Experimental setup of connection between electrode array and acquisition board (picture courtesy of UNIVPM).

It is worthy to underline the importance of positioning such sensors in correspondence of the structural points more subjected to external loads and, hence, possibility of being damaged. For this reason, the electrode array was installed aligning the 4 electrodes with the specimen longitudinal midline, which is the most stressed area, subjected to crack formation.

After the sensors positioning, the preparation of the moulds was finalized inserting two pieces of polystyrene, properly distanced by each other, to cast two specimens (with a 23 cm-length) exploiting the same mould (Figure 23).



Figure 23 Mould with PVC tubes and polystyrene pieces (picture courtesy of UNIVPM).

Through the PVC tubes there were positioned:

- Steel rebar properly deprived from rust (Figure 24).
- 4-electrode array.
- Pseudo-reference array (TiMMO electrode, Figure 25).

According to the scheme given in Figure 26.



Figure 24 Positioning of steel rebars within the mould (picture courtesy of UNIVPM).



Figure 25 Mould with electrode array, TiMMO electrode, and steel rebars (picture courtesy of UNIVPM).

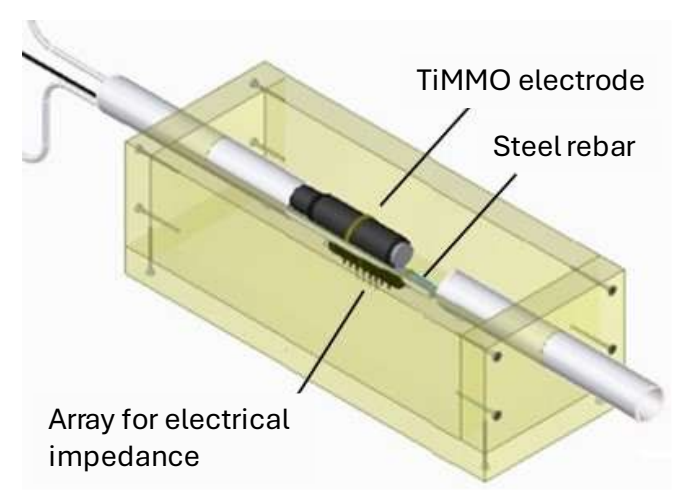


Figure 26 Installation scheme of sensors in the cementitious beam (picture courtesy of UNIVPM).

The sensor installed in the cementitious element to measure the free corrosion potential of the rebar is an activated titanium pseudo-reference electrode: the TiMMO (titanium activated with mixed metal oxides enriched with iridium) electrode, manufactured by Cescor S.r.l. (Figure 27).

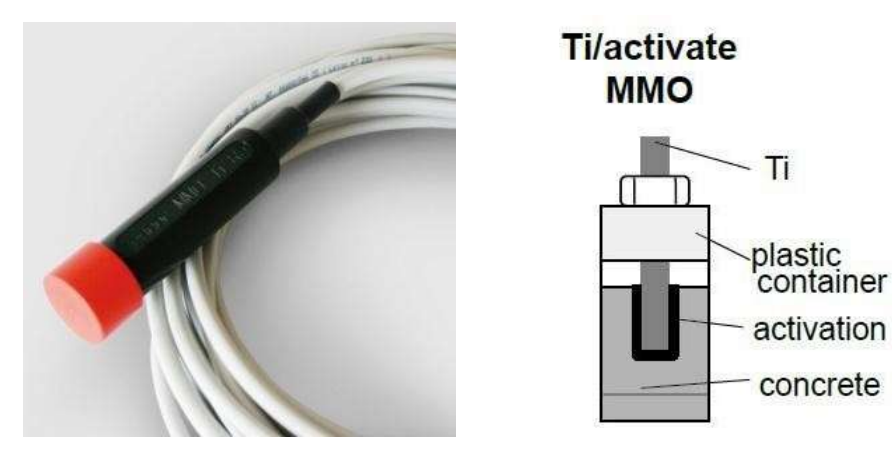


Figure 27 TiMMO pseudo-reference electrode.

The free corrosion potential is an electrochemical parameter indicating the corrosion probability of a reinforcement in a concrete exposed to a certain environment. However, the measured value depends also on the water content/conductivity of the cement-based matrix where the reinforcements is. For this reason, the monitoring of this parameter helps in evaluating the reinforced concrete health status. The Co.S.Mo.Net (Concrete Structures Monitoring Network) is a measurement system (Figure 28), patented by Università Politecnica delle Marche (patent n. 0001364988), for the measurement of free corrosion potential of embedded rebars. It records the signals perceived by the sensor embedded during casting in correspondence of the most critical points of the structural element, that is in the areas more prone to cracking or subjected to degradation and damages due to thermal/hygrometric shrinkage or fatigue. It can be considered effective and low-cost and it provides a significant contribution to the continuous assessment of reinforced concrete structures durability (Tittarelli et al.).

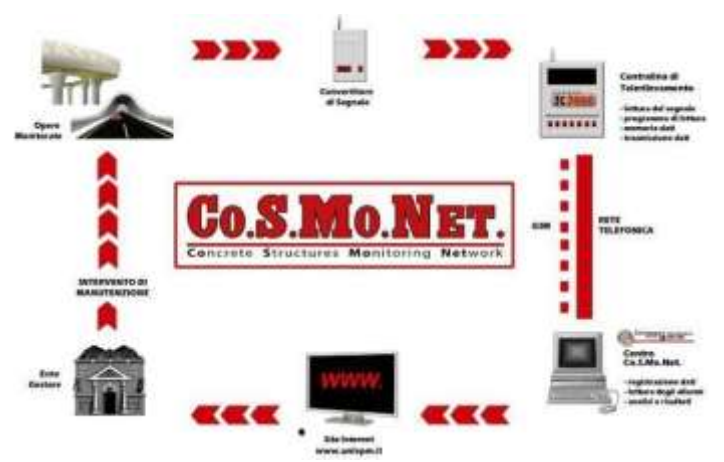


Figure 28 Co.S.Mo.Net monitoring system (picture courtesy of UNIVPM).

To acquire free corrosion potential measurements, it was necessary to install a board and connect it with the cable of the rebar and the cable of the embedded TiMMO pseudo-reference electrode. The board chosen is a STM32 Nucleo-G491RE, which connections are given in Figure 29.

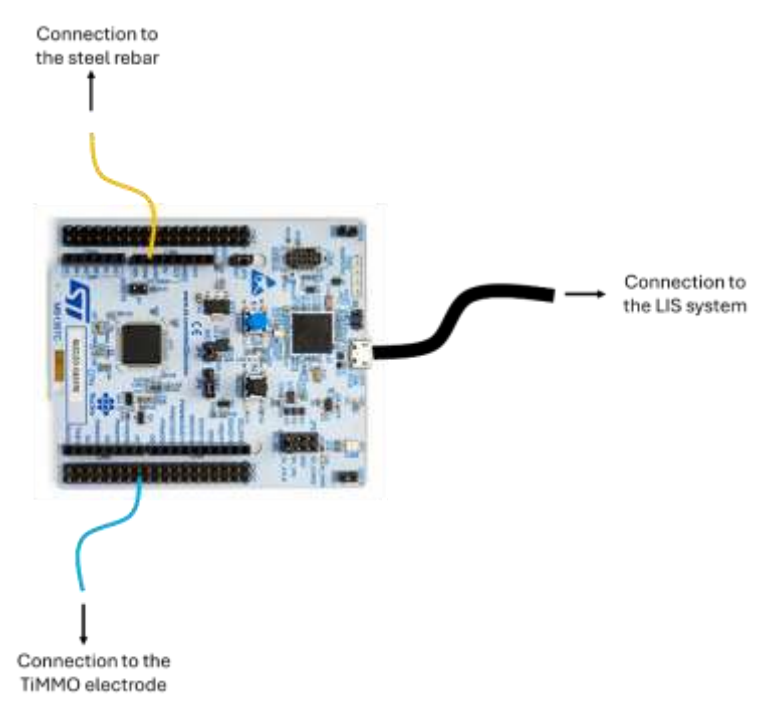


Figure 29. Scheme of the connection of the STM32 Nucleo-G491Reboard for acquisition of free corrosion potential (picture courtesy of UNIVPM).

After the positioning of all elements inside the wooden mould, the casting phase was started, according to the mix-design reported in Table 3.

Table 3. Mix design of the mortar for sensorized blocks.

MIXTURE	CEMENT (G/L)	GNP (G/L)	BCH (G/L)	RCF (G/L)	s.s.a sand (g/l.)	Water (G/L)	W/C RATIO
OPC BCH+RCF	505	-	10	1	1400	303	0.60

The two sensorized specimens just poured in the mould are showed in Figure 30.



Figure 30 Specimen just after the pouring phase (pictures courtesy of UNIVPM).

After casting, the specimens were covered with plastic sheets to avoid water evaporation and cured at room conditions (temperature of 20 $^{\circ}$ C). The PVC tubes were removed 6 hours after casting. After 7 days, specimens were demoulded and left to cure at room conditions.

These two blocks, sensorized as described above, will be installed in the Italian pilot in Camerino, Italy, for SHM purposes (this will be done within the framework of T11.1 Demonstration of the MULTICLIMACT framework at the building scale. The signals coming from the sensorized blocks will be measured through the embedded sensors, which were successfully integrated in the LIS platform, which allows to acquire, store, and pre-process the signals. Indeed, before the on-site installation, the correct functioning of the monitoring platform was verified through laboratory tests conducted in the LIS' offices (Ancona, Italy) for a prolonged period (i.e., February-June 2025). Initially, criticalities arose due to the interferences between the sensors for the measurement of electrical impedance and free corrosion potential. UNIVPM and LIS resolved this issue by employing a hub allowing to do the measurement separately in time, hence avoiding interference and ensuring the quality of the data acquired. Afterwards, it was necessary also to implement a relay in the system, which permits to swich on and swich off alternatively the two sensors and avoid interferences. Such an activity was performed in strict collaboration with T10.2 "Digital solution for the multi-purpose monitoring of environmental and structural behaviour of buildings - development for the application to a real demo case". The detailed results from such tests are reported in the following sections.

4.2. LABORATORY TESTS

The mechanical performance of the innovative self-sensing mortar was tested after 1, 7, and 28 days of curing. The results show that the compressive strength of the mortar increases in time, as expected, and after 28 days reaches its maximum achieves the value of 31 MPa (Figure 31). This value is in line with the previous tests conducted on the same mix and reported in the deliverable D3.3 "Review, design and specifications of cutting edge, evolutive, self-sensing and multifunctional materials and technologies for improving the resilience of buildings, including cultural heritage". This confirms the good reproducibility of the mechanical properties of the patented self-sensing material.

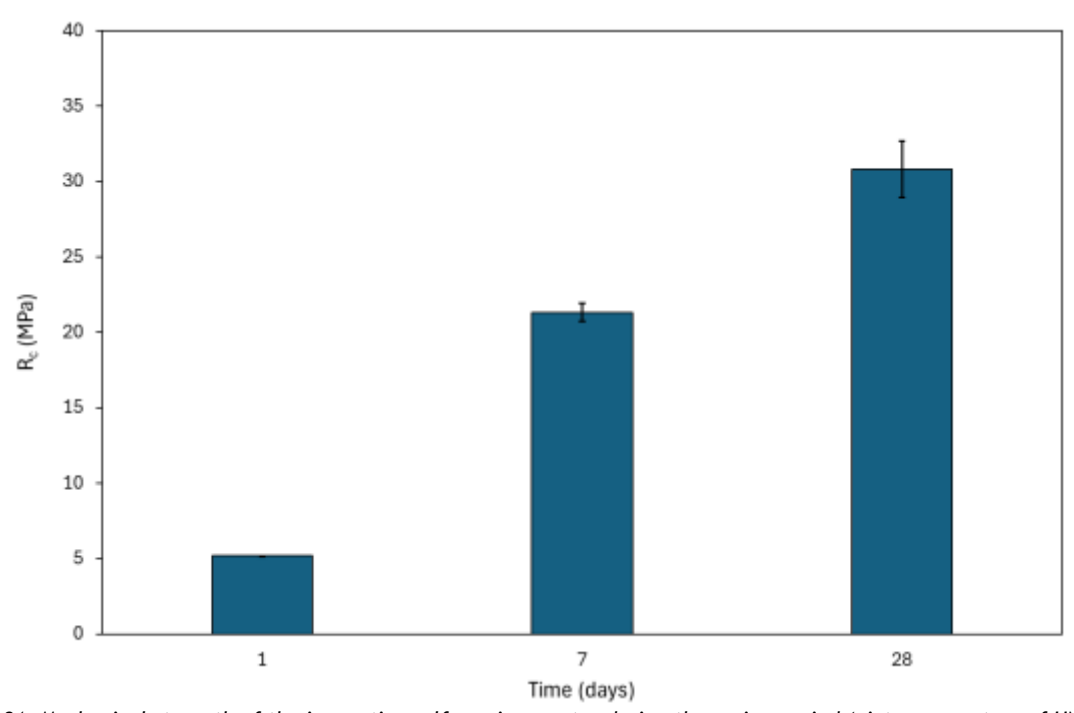


Figure 31. Mechanical strength of the innovative self-sensing mortar during the curing period (pictures courtesy of UNIVPM).

After 28 days of curing, ECCs blocks were brought to the LIS' office, in order to start the acquisition of both electrical impedance and free corrosion potential measurements. The sampling frequency of the EVAL-AD5940BIOZ board is 20 Hz, while the sampling frequency of the STM32 Nucleo-G491RE board is 1 Hz. After a preliminary testing campaign, it was found that the two sensors embedded inside the blocks were not acquiring data correctly. Therefore, an external hub was installed to overcome this problem and the first set of data was discarded. After the hub installation, measurements were started again and acquired in the LIS' platform (in strict collaboration with T10.2). Here, measurements were saved every 30 s (sampling frequency equal to 2 Hz). Acquired data are reported in terms of electrical impedance modulus and phase both for the first (Figure 32) and second (Figure 33) ECCs blocks as well as free corrosion potential of embedded rebars for the first (Figure 34) and second (Figure 35) ECCs blocks. The monitoring of all parameters started on the 1st of February 2025 and ended on the 23rd of June 2025. Data acquisition proceeds very smoothly, but after some months again the electrical impedance was affected by the acquisition of free corrosion potential. Therefore, on the 6th of June 2025 a relay was installed externally in order to switch on and switch off the two sensors alternatively and avoid interferences between them. After the installation of the relay, all the measured data change their value. Indeed, the electrical impedance shifts towards lower values (from 2700 Ω to 1200 Ω for the first block and from 3000 Ω to 900 Ω for

the second block) and the phase moved to -25° and -8° for the two blocks (Figure 32 and Figure 33). Regarding the free corrosion potential values, after the 6th of June 2025 (date of installation of the relay) the values moved from -20 mV/TiMMO to -40 mV/TiMMO and from -50 mV/TiMMO to -25 mV/TiMMO for the first and the second blocks, respectively. As it is possible to notice, the measurements of electrical impedance were much more affected by interferences than free corrosion potential, given that the changes in values were more pronounced for the former compared to the latter. Despite this, it is worthy to note that the parameter of interest is the change in the normal trend of the signal and not in its absolute value and this can be observed also in case of interferences. However, to have a more accurate measurement is always preferrable and with the final configuration, possible interfering factors have been minimized. After the 23rd of June 2025, both blocks were disconnected by the LIS' platform to begin the preparation of the measuring system and materials for the Italian pilot.

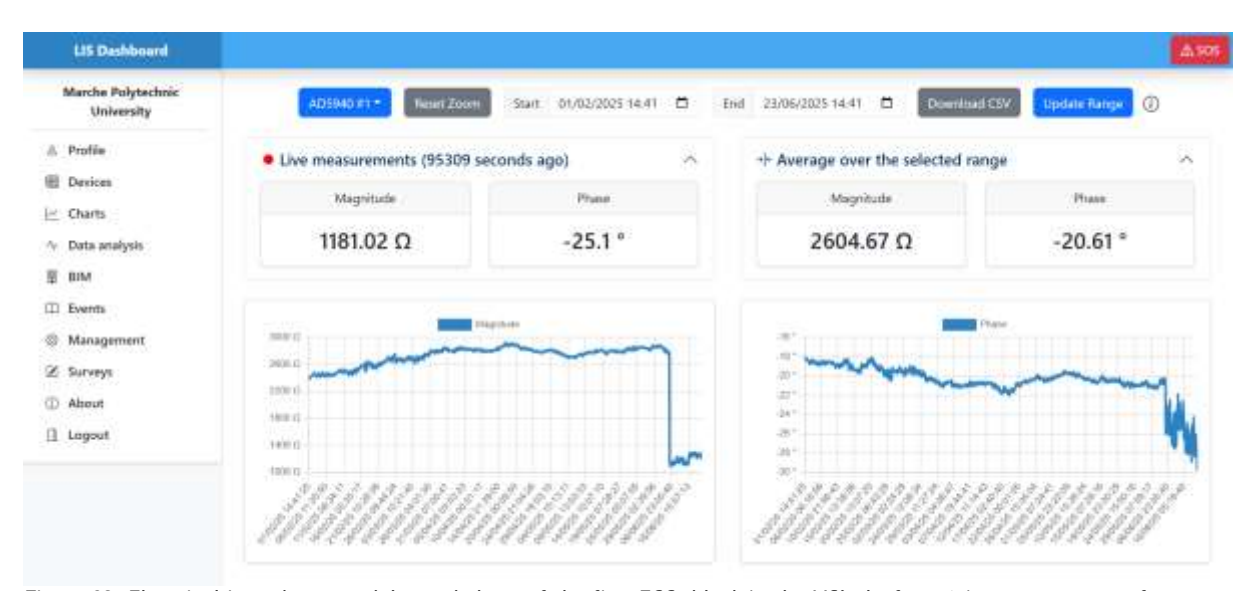


Figure 32. Electrical impedance modulus and phase of the first ECCs block in the LIS' platform (pictures courtesy of UNIVPM).

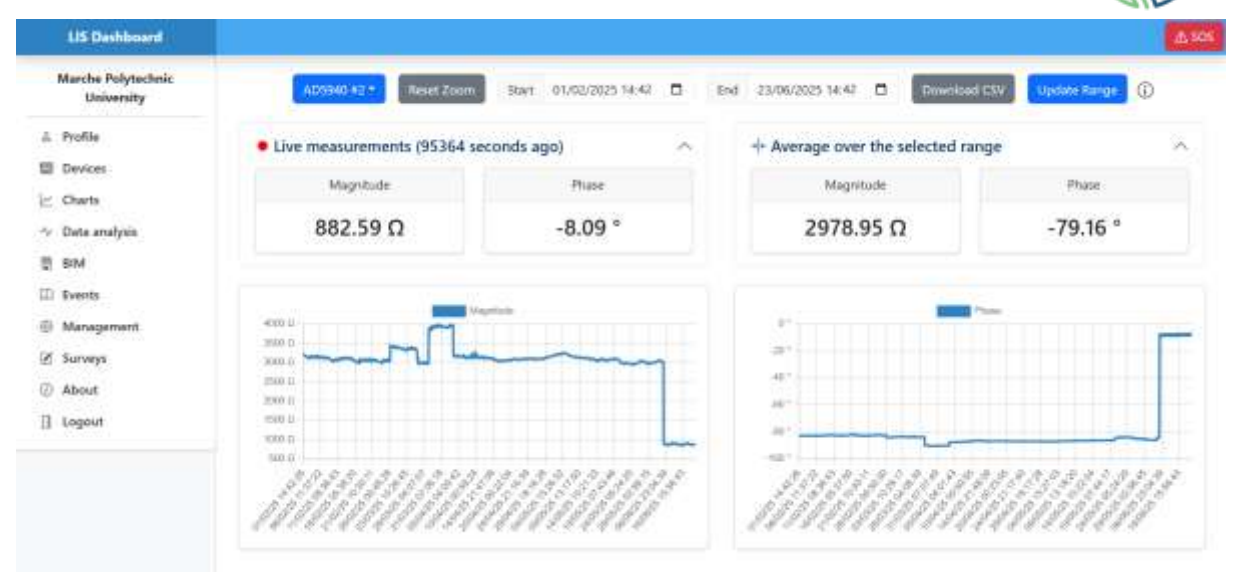


Figure 33. Electrical impedance modulus and phase of the second ECCs block in the LIS' platform (pictures courtesy of UNIVPM).

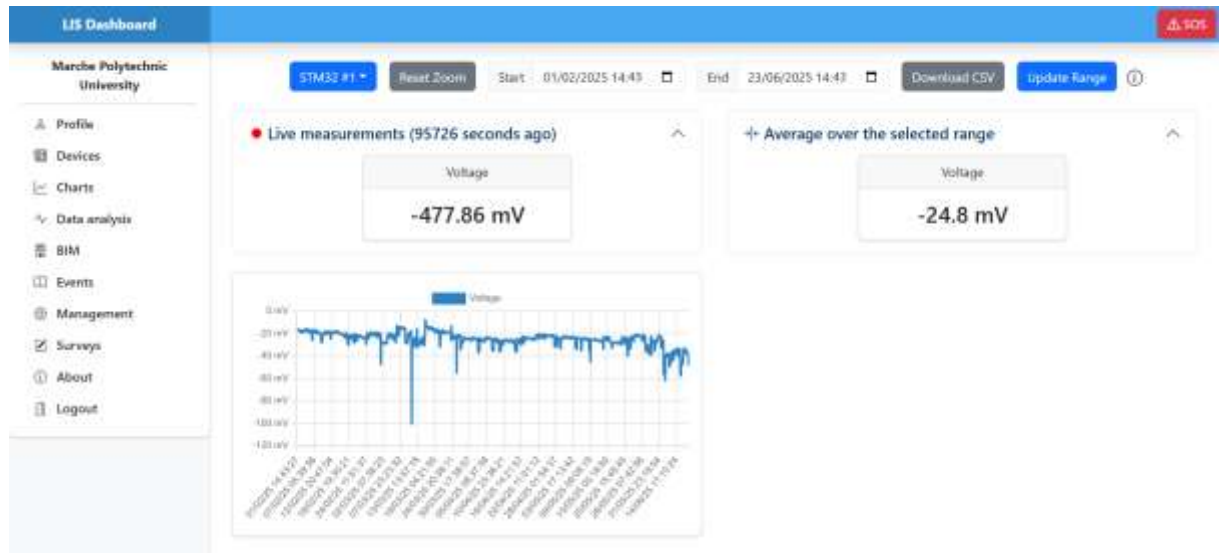


Figure 34. Free corrosion potential of the embedded rebar of the first ECCs block in the LIS' platform (picture courtesy of UNIVPM).

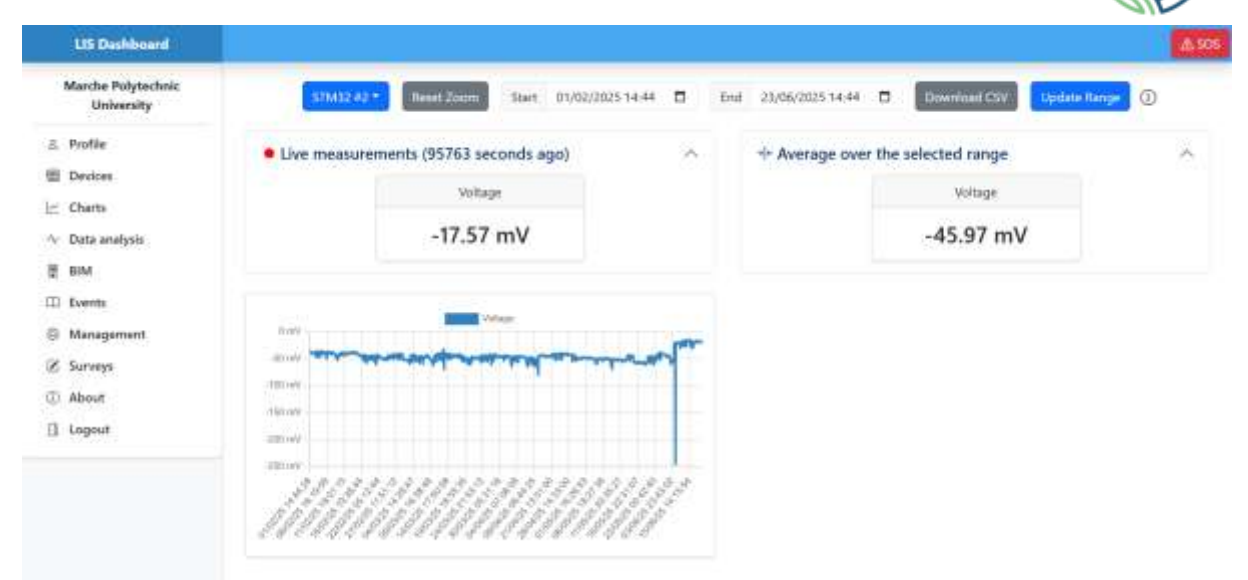


Figure 35. Free corrosion potential of the embedded rebar of the second ECCs block in the LIS' platform (picture courtesy of UNIVPM).

4.3. PREPARATION OF THE ITALIAN PILOT

UNIVPM, in collaboration with LIS, planned and executed all the preparatory activities for the Italian pilot. These included the following:

- Assembly of the monitoring system, comprising software configuration and hardware connections.
- Preliminary tests execution in the LIS facilities for indoor multidomain comfort assessment. The test protocol was developed in collaboration with UKA within the framework of T8.5 Human-centred built environment design for improving people health and well-being-development for the application to a real demo case.

Part of the results obtained from these activities have been described in two conference contributions, namely:

- G. Cosoli et al., Development of a BIM-Based Platform for the Assessment of Indoor Multidomain Comfort. IEEE MetroLivEnv 2025, June 2025, Venice, Italy. This contribution is focused on the description of the whole methodology developed for the assessment of indoor multidomain comfort, including the selection of proper sensors, the processing pipeline, and the digital platform used to implement the tests.
- G. Cosoli et al. (2025) A Measurement Approach for the Assessment of Indoor Multidomain Comfort: the MULTICLIMACT Experience. IEEE MetroXRAINE 2025, October 2025, Ancona, Italy. This contribution described the results from the preliminary tests conducted in the LIS facilities (Ancona, Italy) in preparation to the experimental campaign to be carried out in the pilot building in Camerino, Italy.

In June 2025, the two ECCs sensorized blocks have been installed in the ex-Carmelitane building, located in Camerino (MC), Italy, which geographical coordinates are 43°08'16.1"N 13°04'08.5"E (Figure 36). The Italian pilot consists of two twin rooms with similar orientation (Figure 37) and dimensions (Figure 38).



Figure 36. Google Maps view of the location of the Italian demo.

The room selected for the in-field monitoring of electrical impedance and corrosion potential of embedded rebar embedded inside the two ECCs blocks is located at the first floor of the building, with a south-west orientation (Figure 37). The room, labelled as Twin Room 2 in Figure 38 is used as an office, with dimensions of $2.40 \text{ m} \times 3.72 \text{ m}$ and height of 3.27 m.



Figure 37. Façade view of the two twin rooms chosen for the Italian pilot in the ex-Carmelitane building (pictures courtesy of UNICAM).

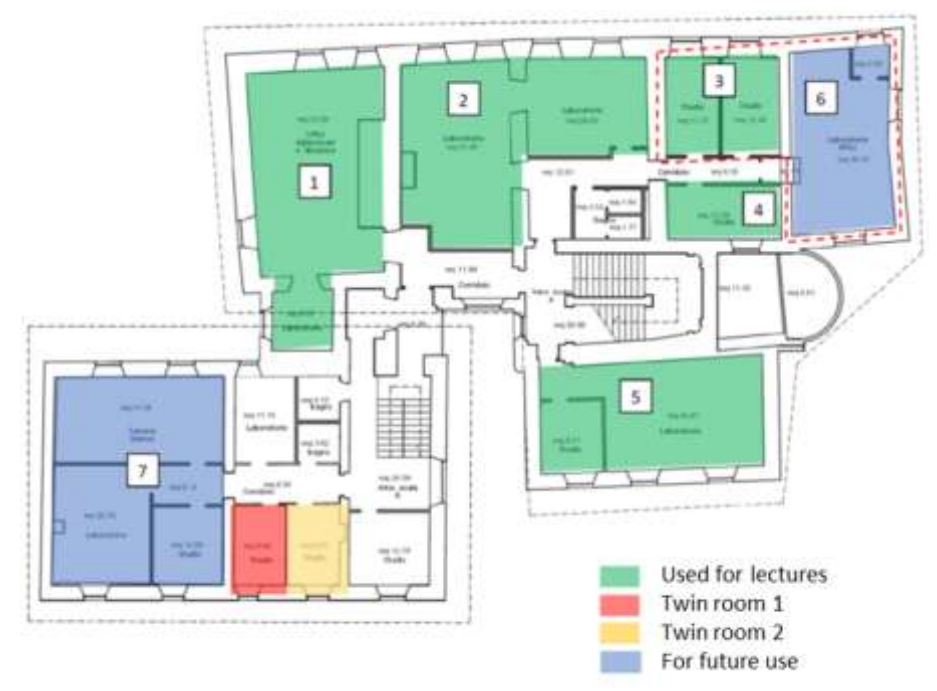


Figure 38. Plan of the first floor of the ex-Carmelitane building (pictures courtesy of UNIVPM).

The two blocks were installed inside a recess opened in the existing wall, as reported in Figure 39. The blocks were placed on the floor and a contrast system was applied on them to simulate the weight of the above wall. The niche will be closed by plasterboards where a small door will be fabricated in order to permit possible inspections during the whole test duration. The blocks will be connected to

a monitoring system, developed by LIS, which through the LIS' platform itself will acquire and store both electrical impedance and corrosion potential signals during the in-field testing campaign.



Figure 39. Recess opened in the existing wall with ECCs blocks on the floor (pictures courtesy of UNIVPM).

5. DEVELOPMENT OF MULTIFUNCTIONAL MORTAR PANELS FOR INDOOR AIR QUALITY IMPROVEMENT

The growing demand for more comfortable and healthier indoor environments, along with the need for energy-efficient buildings, calls for new strategies such as the development of passive systems that can complement active technologies like air conditioners, purifiers, and dehumidifiers currently used to enhance indoor air quality (IAQ) (Pierpaoli et al.; González-Martín et al.). In this context, finishes applied to interior walls and ceilings, due to their large area exposed to the indoor environment, can play a significant role in passively improving IAQ (Zuraimi et al.; Ren et al.; Bahri et al.; Kunkel et al.). Finishes applied on walls and ceilings, covering extensively indoor surfaces, are able to reduce indoor pollution and contribute to ameliorate the health and well-being of occupants. In this context, the multifunctional mortar developed by UNIVPM (patent n. 102017000033750), being prepared with highly porous aggregates and photocatalytic agents, has reported to be able to passively decrease the concentration of pollutants (e.g. VOCs) and regulate the indoor RH. It has also demonstrated to be efficient both at laboratory (TRL 4) and at pilot (TRL 6) scales (Giosuè, Czerwinska, et al.).

During the first 12 months of the MULTICLIMACT project (first reporting period), the UNIVPM multifunctional mortar was applied to a natural hemp-based panel to develop a sustainable multilayer system able to improve the thermal comfort. The results were compared with other 3 multilayer systems, including those based on petrochemical materials and reported in the D3.3 "Review, design and specifications of cutting edge, evolutive, self-sensing and multifunctional materials and technologies for improving the resilience of buildings, including cultural heritage". During the following 12 months of the MULTICLIMACT project (second reporting period), the innovative multilayer system has been optimized since it was found that the natural-based panel initially chosen as substrate for the UNIVPM multifunctional mortar was not compatible with. Therefore, mechanical tests were repeated with another type of hemp-based panel and the performance of the novel multilayer system was also evaluated in terms of permeability to water vapour, moisture buffering value, and depolluting activity.

5.1. OPTIMIZATION OF THE MULTILAYER PANELS

During the experimental campaign carried out within WP3 T3.3 (M1-M12) some criticalities have raised. Indeed, the hemp-based panel (Canapannel 100) coupled to the layers of Canapamix 3 and UNIVPM multifunctional mortars gave mould growth and panel deformation due to shrinkage of UNIVPM mortar related to water evaporation. Shrinkage of UNIVPM mortar induced also cracks formation on its surface since the moduli of elasticity of the panel, the Canapamix 3 mortar and the UNIVPM finish were different. Additionally, the Canapamix 3 substrate emitted a strong odour during the mixing procedure, probably related to a high emission of VOCs, which could represent a serious problem for the subsequent demosite indoor tests for the health of occupants. All these criticalities have been already reported within the D3.3 "Review, design and specifications of cutting edge, evolutive, self-sensing and multifunctional materials and technologies for improving the resilience of buildings, including cultural heritage".

Therefore, within the Task 9.3 (M13-M24) the natural-based materials chosen both for the panel and the mortars substrate, i.e., Canapannel 100 and Canapamix 3, have been substituted with other hemp-based materials. In details, the chosen new panel is a hydraulic lime-based hemp panel commercialized as "pannello LHP" and the hemp-based substrate mortar is a hydrated lime-based one commercialized as "Rasante per LHP", both produced by BIOmat canapa (Pedone working S.r.l., Foggia, Italy, https://biomatcanapa.it/). As reported in the technical datasheet, the hemp-based panel has a density of 350-400 kg/m³, a resistance to water vapour coefficient (µ) of 4.5 and a thermal

conductivity (λ) of 0.06-0.07 W/(m·K). The "Rasante per LHP" mortar has an apparent density of 1.7 g/cm³, $\mu \le 20$ (according to EN 1745), and λ of 0.47 W/(m·K) (according to EN 1745), as reported in the technical datasheet. Given the lower thickness of the new hemp panel (30 mm) compared to the Canapannel 100 and the XPS one of the previous experimentations (40 mm), the test campaign was replicated also for the commercial system based on XPS with 30 mm thickness in order to compare better the results obtained from the petrochemical and natural systems. In this new set of tests, also the Keradecor Paint was substituted by another one commecialized as "Iris Color" by Iris Color S.r.l. (San Giuliano Milanese, Italy, https://iriscolor.eu/) that requires its own fixative to be applied on other mortar substrates.

The new mortar substrate (Rasante per LHP) was prepared according to the mix design reported in Table 4.

Table 4. Mix-design and workability of Rasante per LHP mortar in g/L.

MXTURE	WATER (G/L)	PREMIXED MORTAR (G/L)	WATER/BINDER RATIO	SLUMP (MM)
Rasante per LHP	252	935	0.27	118

During casting, the workability was tested with a flow table test according to the UNI EN 1015-3 (EN 1015-3:1999/A2:2006 - Methods of Test for Mortar for Masonry - Part 3: Determination of Consistence of Fresh Mortar (by Flow Table)) and UNI EN 1015-6 (EN 1015-6:1998/A1:2006 - Methods of Test for Mortar for Masonry - Part 6: Determination of Bulk Density of Fresh Mortar) standards. Results indicate stiff workability for the mortar (Table 4). Then, mortars were poured into 40 mm x 40 mm x 160 mm prismatic moulds, put inside a climatic chamber at temperature (T) of 20 \pm 1 $^{\circ}$ C covered with plastic film to ensure a relative humidity (RH) ≥ 95%. After 2 days of curing, mortars were demoulded and covered again with plastic for further 5 days. Then, the plastic cover was removed, and specimens were left to cure inside the climatic chamber at RH = $50 \pm 5\%$ for 28 days. Mortars were tested in terms of compressive strength (R_c) after 28 days of curing according to the EN 1015-11 standard (EN 1015-11:1999/A1:2006 - Methods of Test for Mortar for Masonry - Part 11: Determination of Flexural and Compressive Strength of Hardened Mortar) on three specimens per composition with a Galdabini hydraulic press (Cardano al Campo, Italy, https://www.galdabini.it/) with 400 kN full scale. After 28 days of curing, before compression, also the dynamic modulus of elasticity (E_d) was measured on the same three prismatic specimens per composition according to the UNI EN 12504-4 (EN 12504-4:2004 -Testing Concrete in Structures - Part 4: Determination of Ultrasonic Pulse Velocity) with the PUNDIT device as reported in "D3.3 - Review, design and specifications of cutting edge, evolutive, self-sensing and multifunctional materials and technologies for improving the resilience of buildings, including cultural heritage".

The different systems based on the coupling of panels, substrates and finishes were prepared according to the 4 different combinations reported hereafter:

- 1) XPS+PAINT: SOPRAXPS + Mapetherm + Rasobuild + Iris Color paint
- 2) XPS+UNIVPM: SOPRAXPS + Mapetherm + Rasobuild + UNIVPM multifunctional mortar
- 3) HEMP+PAINT: Pannello LHP + Rasante per LHP + Iris Color paint
- 4) HEMP+UNIVPM: Pannello LHP + Rasante per LHP + UNIVPM multifunctional mortar

In Figure 40 the 4 different combinations with the height of each layer are reported. The application of the different layers and the timing of casting was the same reported in "D3.3 - Review, design and specifications of cutting edge, evolutive, self-sensing and multifunctional materials and technologies for improving the resilience of buildings, including cultural heritage".

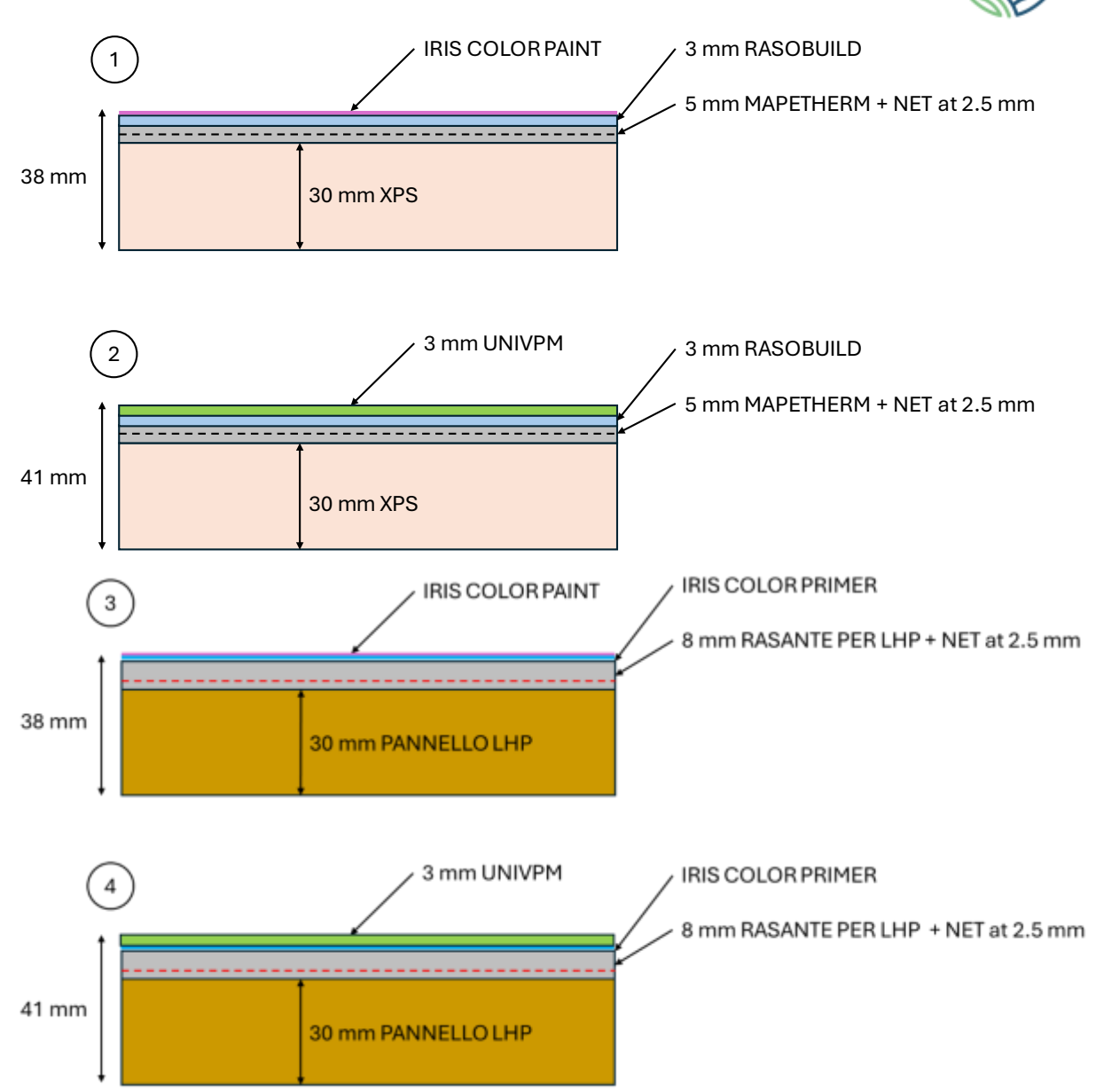


Figure 40. The four tested multilayer panel combinations (pictures courtesy of UNIVPM).

The procedure followed to apply each mortar layer and finishing is the same reported in D3.3 "Review, design and specifications of cutting edge, evolutive, self-sensing and multifunctional materials and technologies for improving the resilience of buildings, including cultural heritage".

5.2. LABORATORY TESTS

Mechanical results of mortars after 28 days of curing are reported in Table 5. For commercial mortar substrates, the results of compressive strength are slightly different from those reported in the technical datasheet, indeed R_c values of Mapetherm and Rasobuild are approximately 20% lower. Conversely, Rasante per LHP is in line with the technical datasheet, indeed it has a Rc similar to that of CS II mortars (2.5 MPa) according to the EN 1015-11. Concerning the dynamic modulus of elasticity,

it can be stated that all mortars had a very low stiffness. Conversely, the results obtained by the UNIVPM multifunctional mortar are in line with those by previous experimentations.

Table 5. R_c and E_d values of Mapetherm AR1 GG, Rasobuild Eco Extrafino, Rasante per LHP, and UNIVPM ma	Table 5. R_c and E_d values
--	---------------------------------

MXTURE	Rc (MPA)	E₀ (GPa)
Mapetherm AR1 GG	4.6 ± 0.8	8.6 ± 0.1
Rasobuild Eco Extrafino	2.1 ± 0.2	4.5 ± 0.1
Rasante per LHP	2.6 ± 0.2	8.1 ± 0.4
UNIVPM	4.1 ± 0.3	5.8 ± 0.2

The results obtained by the adhesion to substrate test are reported in Table 6. As it is possible to notice, XPS and HEMP substrates give the same results, regardless of the multilayer systems applied on them. In particular, concerning the XPS panel all failures occurred on the interface with Mapetherm (fracture type "a", Figure 41) or Rasobuild and Mapetherm substrates (fracture type "a", Figure 42), meaning that the UNIVPM multifunctional mortar has a higher adhesion strength than that of the other substrate mortars. Also, for HEMP-based systems the failure mechanisms occurred always on the hemp/substrate interface (fracture type "a", Figure 43 and Figure 44) with very low f_u values.

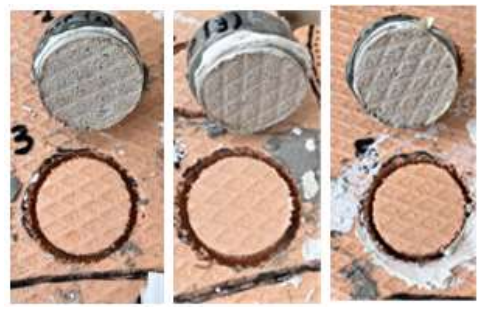


Figure 41. Failure mechanisms of XPS+PAINT (pictures courtesy of UNIVPM).



Figure 42. Failure mechanisms of XPS+UNIVPM (pictures courtesy of UNIVPM).



Figure 43. Failure mechanisms of HEMP+PAINT (pictures courtesy of UNIVPM).



Figure 44. Failure mechanisms of HEMP+UNIVPM (picture courtesy of UNIVPM).

Table 6. f_u values of the 4 multilayer systems.

MULTILAYER SYSTEM CODE	MULTILAYER SYSTEM	Fu (MPA)
1	XPS+PAINT	0.15 ± 0.03
2	XPS+UNIVPM	0.09 ± 0.02
3	HEMP+PAINT	0.01 ± 0.00
4	HEMP+UNIVPM	0.02 ± 0.00

The hygrometric properties of the multilayer panels have been evaluated both in static and dynamic conditions, in terms of water vapour resistance factor (μ) and Moisture Buffering Value (MBV), respectively.

The water vapour permeability was tested according to the EN 1015-19 on cylindrical specimens with a diameter of 168 mm. On the other hand, the MBV defines the humidity absorbed and desorbed by the material on the surface unit when it is placed in an environment at RH of 75% for 8 hours and of 33% for 16 hours, according to a simplified procedure of NORDTEST (Giosuè, Pierpaoli, Mobili, et al.). For each combination, the average MBV calculated over 3 cycles was obtained. The tested specimens had an area of 150 mm x 150 mm with the lateral surface previously sealed with silicone to guarantee a homogeneous water vapour flow. Before starting the test, specimens are pre-cured at a temperature of 20 ± 1 °C and RH of $50 \pm 5\%$ for 24 hours inside a climatic chamber. The practical MBV [g/(m²% RH)] was calculated as the amount of moisture changed by the material per surface unit and RH gradient, as indicated in (Mazhoud et al.), and reported in equation (1):

$$MBV = \frac{G}{\Delta RH}$$
 (1)

where G is the absorbed humidity [g/m²] and ΔRH is the variation of relative humidity [%]. The test ends when at least 3 mass variation measured at the same RH have a difference < 5%. The results of the water vapour permeability of the four multilayer panels in terms of μ value are given in Figure 45. As expected, both XPS+PAINT and XPS+UNIVPM obtained very high μ values of 56.9 and 42.3, respectively, since the two combinations used a XPS petrochemical panel with μ value of 150, not suitable for the passage of water vapour. Conversely, the two combinations made of HEMP, i.e., HEMP+PAINT and HEMP+UNIVPM, show very low μ values equal to 9.4 and 7.8, respectively; indeed, the hemp-based substrate is much more breathable than XPS, and it is commercialised as a dehumidifying panel having a μ value of 4.5. It is interesting to highlight that the substitution of the paint with the multifunctional UNIVPM mortar as finishing contributes to decrease the resistance to water vapour by 26% and 17% when applied on the XPS and HEMP panels, respectively, making the multilayer combination more breathable.

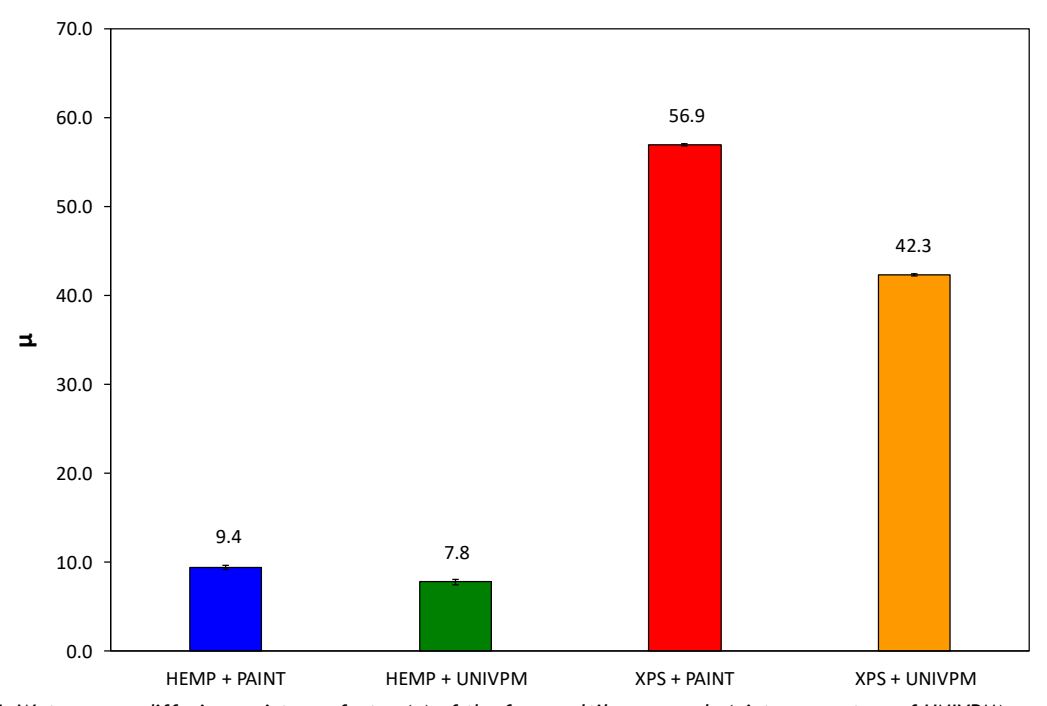


Figure 45. Water vapor diffusion resistance factor (μ) of the four multilayer panels (picture courtesy of UNIVPM).

Results of hygrometric properties of the multilayer panels evaluated in dynamic conditions are reported in Figure 46 and Figure 47. The former reports the trend of water content of the four compositions during the cyclic exposure at RH = 75% for 8 h and at RH = 33% for 16 h in the climatic chamber and the latter the corresponding MBV calculated values. A high MBV value indicates an increased capacity of the material to absorb and release water vapour, by acting as a moisture buffer. The lower MBV value is measured for XPS+PAINT composition, which is equal to 1.16. When the paint is replaced by the multifunctional mortar, the MBV value increases by 58%. Replacing instead XPS with HEMP results in a slightly higher MBV value (+13%) than XPS+PAINT composition. On the other hand, by using HEMP as substrate and the UNIVPM multifunctional mortar as finishing (i.e., HEMP+UNIVPM composition), the MBV of the system increases by 91%. This confirms that the innovative system based on natural-based materials is much more efficient for the regulation of indoor RH.

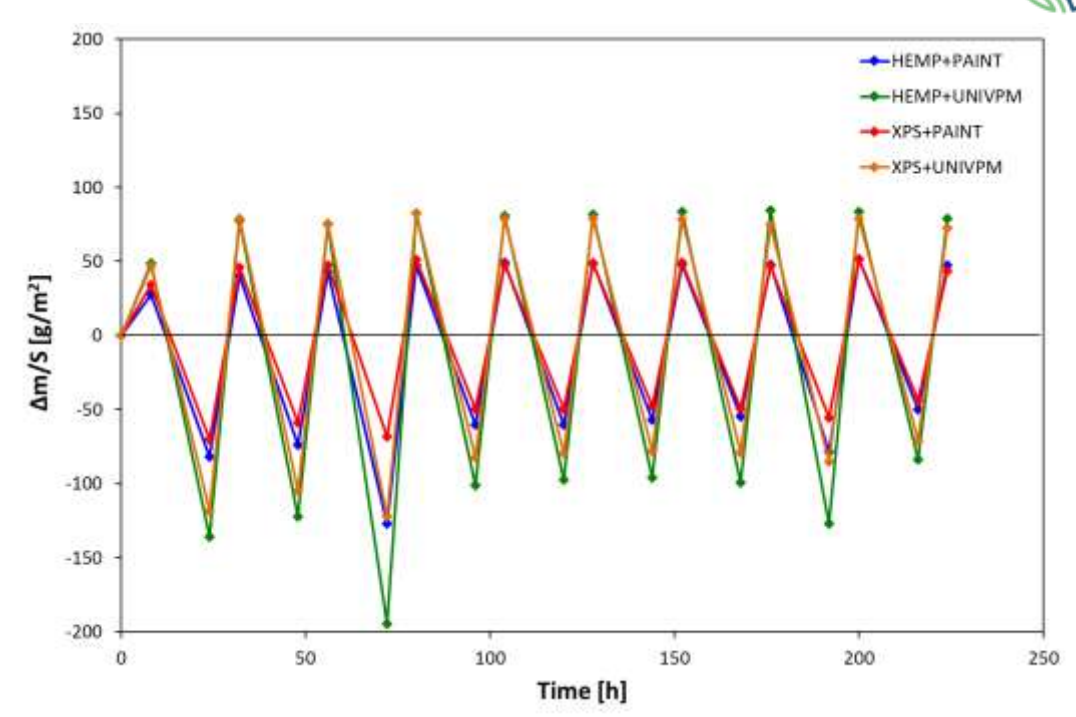


Figure 46. Change in water content of the four multilayer panels during the cyclic exposure at RH = 75% for 8 h and at RH = 33% for 16 h in the climatic chamber (picture courtesy of UNIVPM).

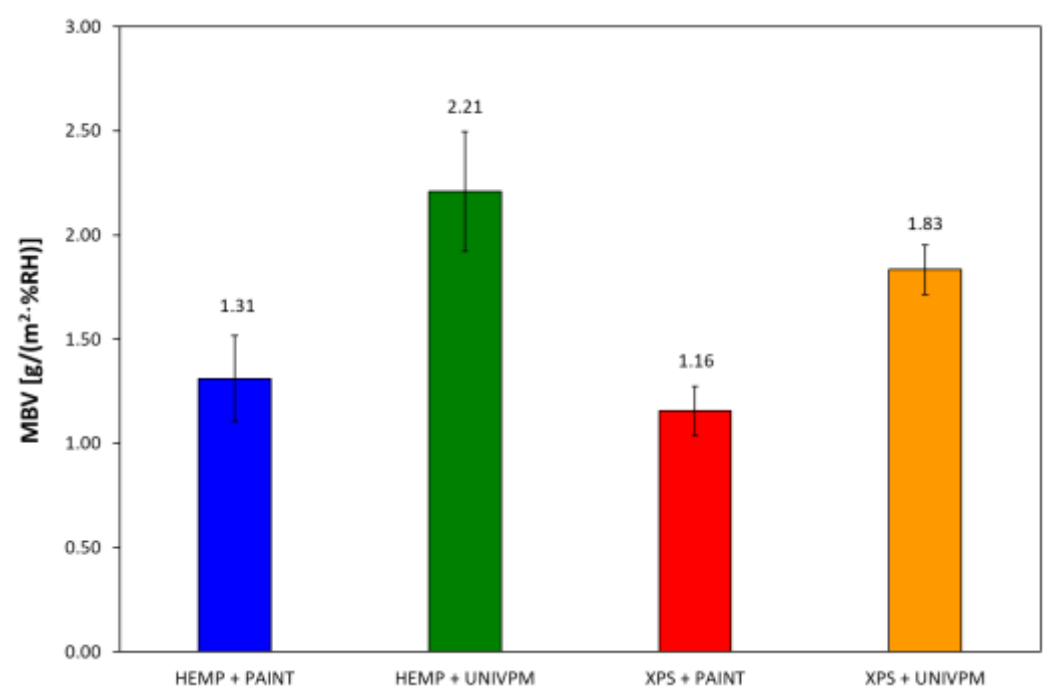


Figure 47. MBV of the four multilayer panels (picture courtesy of UNIVPM).

The depolluting capacity of the 4 combinations of multilayer panels was studied in terms of adsorption and photocatalytic activity on prismatic specimens with a surface area of 70 mm x 70 mm (Giosuè, Czerwinska, et al.). The adsorptive properties were evaluated in batch by using a model pollutant

(i.e., Methyl Ethyl Ketone (MEK)). Before the test, specimens lateral and bottom surfaces were sealed with a metallic tape and dried in oven at 50 °C for 24 hours. Then, each specimen was placed in a glass box of 17 litres equipped with a fan. To obtain inside the box a theoretical initial MEK concentration of 797 ppm, 50 µL of MEK were injected with a micro-syringe from an upper hole hermetically closed with a rubber sept. The MEK concentration inside the box was measured in time with a PID (Photoionization Detector) sensor (Aeroqual Series 900, https://www.aeroqual.com/) connected to a laptop. The photocatalytic activity was measured by following the procedure reported in the UNI 11247 standard, which measures the nitrogen oxides (NOx) degradation rate in plug flow condition. Specimens were tested both under VIS (Philips lamp, 42 W) with intensity equal to 9 ± 1 W/m² as detected by Delta Ohm HD 2101.1 photo radiometer (probe LP471 RAD 400 - 1050 nm), and UV radiation (halogen lamp, 400 W) with measured light intensity of 20 ± 1 W/m2 (probe LP471 UVA 315 - 400 nm). The NOx flux was supplied by a NOx tank (SAPIO S.r.l., Monza, Italy), with a concentration of 500 ± 5 ppb in a dilution flow of 1.5 l/min, and was kept constant by mixing with air at T = 20 ± 2 °C and RH 50 ± 10 % using a dilution system (Calibrator 8188, Rancon Instruments S.p.A., Milan, Italy) continuously monitored in terms of NOx and NO concentrations by a chemiluminescence NOx analyser (nitrogen oxide analyser model 8841; Monitor Labs, Englewood, CO, United States). Each tested specimen was placed in a 3 litres borosilicate reactor and, as soon as the NOx flux was stable, photocatalytic activity (%D) was evaluated following equation (2):

$$\%D = \frac{C(dark)-C(light)}{C(dark)} \cdot 100$$
 (2)

where %D is the percentage of degradation and C(dark) and C(light) are the concentrations of NO or NOx in the dark and light conditions (after 10 min of irradiation), respectively.

Results obtained in terms of VOCs concentration inside the glass box during the test and total VOCs adsorption at the end of the test are reported in Figure 48 and Figure 49, respectively. In the figures, also the blank line is reported, which is the VOCs concentration/adsorption test inside the box without the specimens. As it is possible to notice, when the surface of the multilayer panels is covered by the paint, the VOCs concentration reduces by 43% in the case of HEMP+PAINT and 54% in the case of XPS+PAINT. Conversely, the application of the UNIVPM multifunctional mortar in place of the paint contributes to a much higher reduction in VOCs concentration up to 78%. This confirms the great depolluting ability of the patented mortar, thanks to the presence of the highly porous nonconventional aggregates (Giosuè, Pierpaoli, Citterio, et al.). The photocatalytic activity of the 4 multifunctional panels is reported in Figure 50 and Figure 51, respectively under VIS and UV lights. As expected, in the specimens with commercial finishing (i.e., paint), photocatalytic activity is negligible, given the low removal percentages, since the photocatalytic agents are not present. Conversely, the combinations with the UNIVPM multifunctional finishing are those that have led to a considerable reduction of pollutants, more specifically under UV irradiation. This is because photocatalytic materials such as titanium dioxide require high energy for activation and UV light, thanks to higher frequency and shorter wavelength than visible (VIS) light, has more energy.

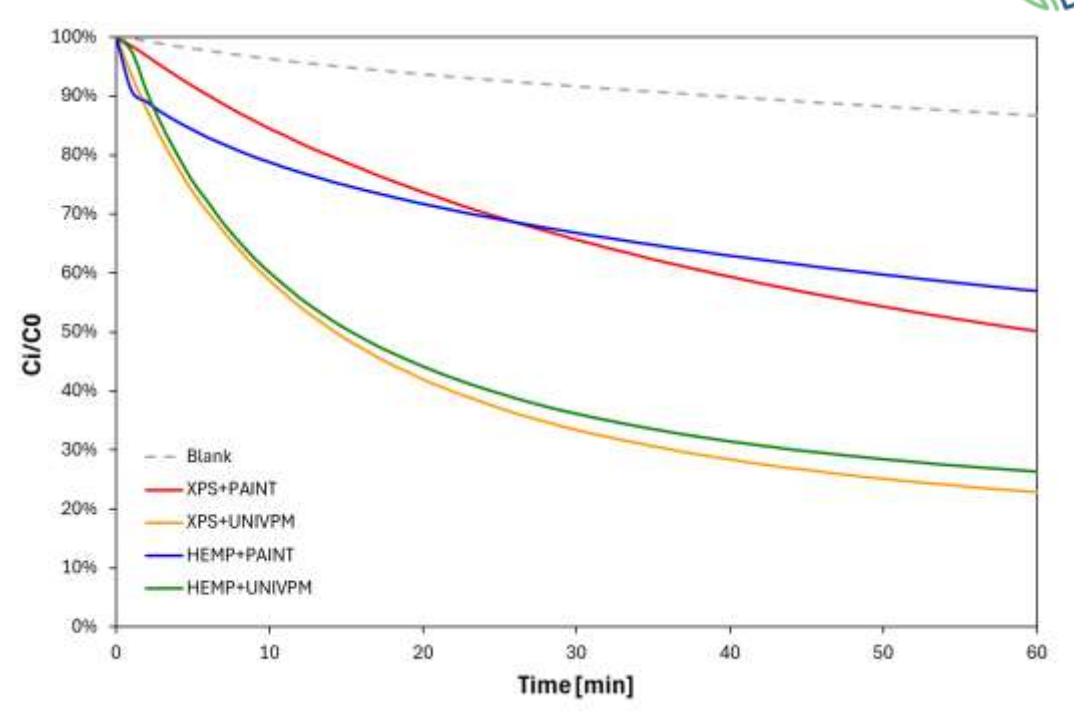


Figure 48. VOCs concentration (%) inside the box with the four multilayer panels (picture courtesy of UNIVPM).

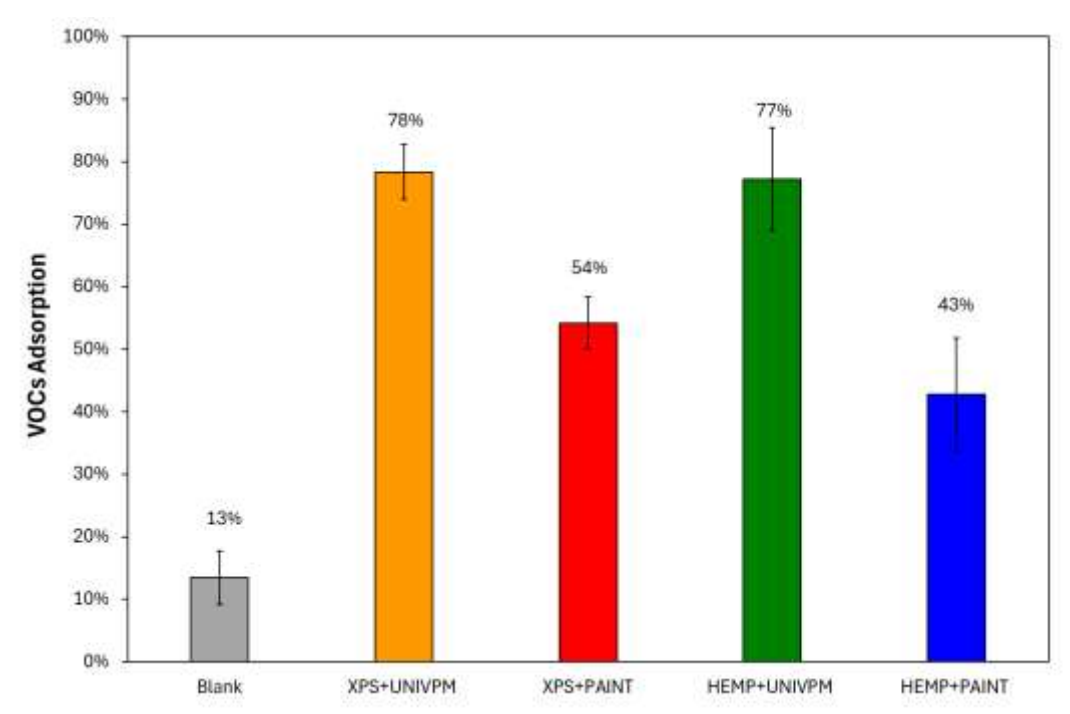


Figure 49. VOCs adsorption (%) of the four multilayer panels (picture courtesy of UNIVPM).

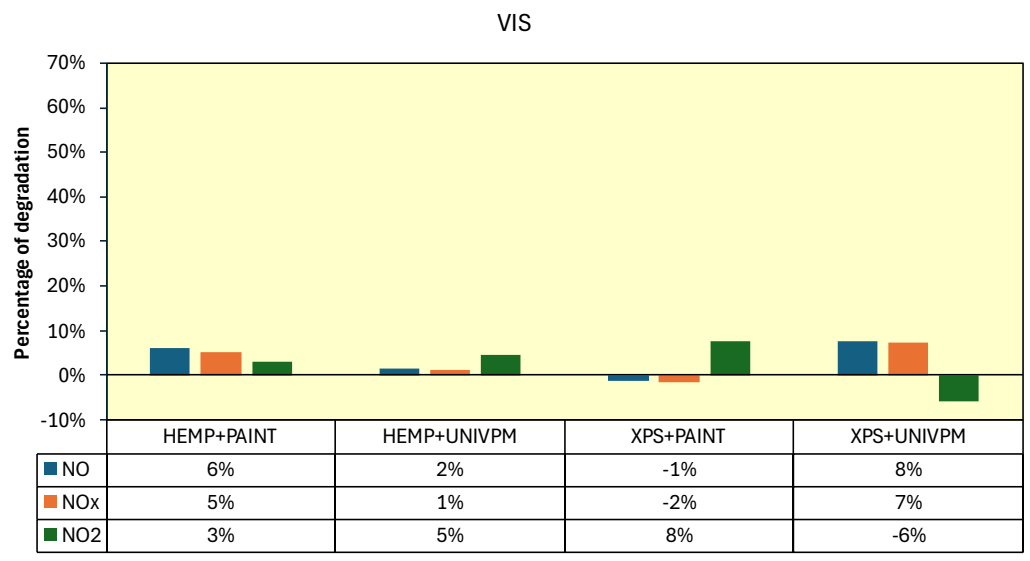


Figure 50. NO, NOx and NO₂ degradations inside the box under VIS light (picture courtesy of UNIVPM).

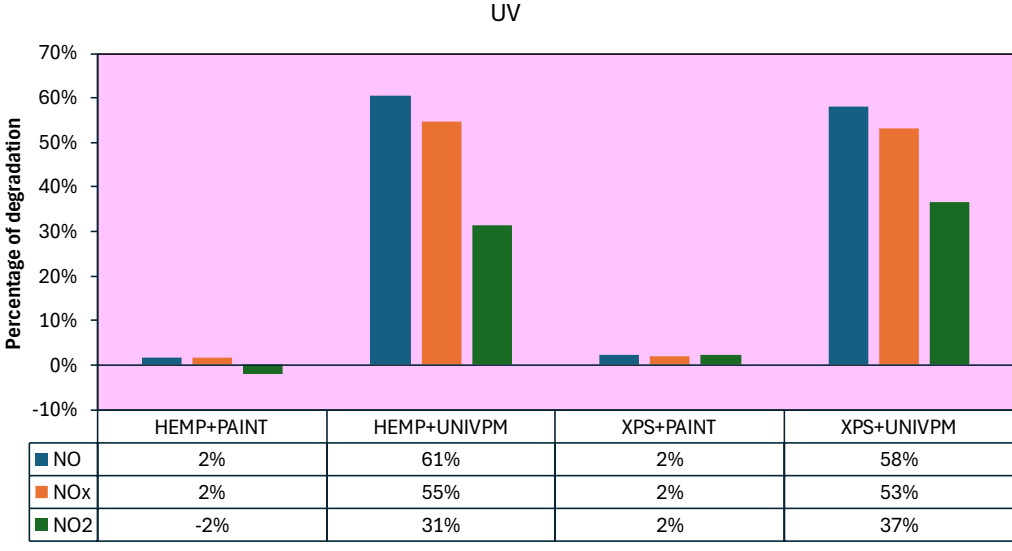


Figure 51. NO, NOx and NO₂ degradations inside the box under UV light (picture courtesy of UNIVPM).

Laboratory tests have confirmed that the most promising multilayer panel is the one based on hemp with the application of the multifunctional UNIVPM mortar. Indeed, this system provided good thermos-mechanical properties and ensures the highest reduction of VOCs and NOx. Moreover, the new hemp-based system was not susceptible of mould formation, highlighting the good inertization of the natural substrate by mineralization. However, the mechanical compatibility of the hemp-based substrate with the patented multifunctional mortar was still an issue. Several cracks developed during the curing of the multilayer system at room conditions, as displayed in Figure 52.

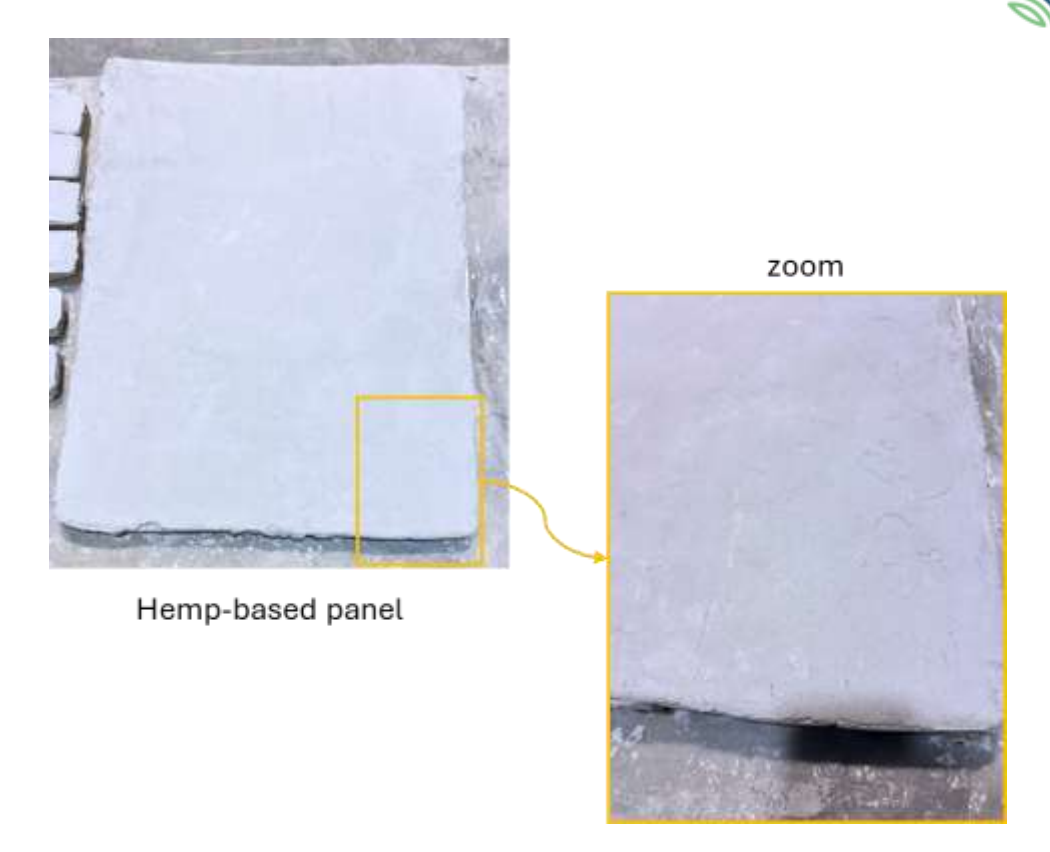


Figure 52. cracks development on the UNIVPM mortar applied on the multilayer natural-based system (picture courtesy of UNIVPM).

For this reason, further tests were conducted to reduce the drying shrinkage of the UNIVPM multifunctional mortar. Four different strategies were tested, all based on the modification of the mix design by also varying the quantity of water in order to obtain always the same stiff workability (< 140 mm):

- Adding 2% of superplasticizer on the mass of powders.
- Adding 1.5% of cellulose fibers on the mass of powders.
- Adding 2.5% of CaO on the mass of hydraulic lime.
- Adding 5% of CaO on the mass of hydraulic lime.

Results of the flow values obtained during casting are reported in Table 7: all mortars have a stiff workability lower than 120 mm. After casting, mortars were cured in the climatic chamber, with the same procedure previously reported. After 28 days of curing Table 7all five mortars showed similar compressive strength values (Table 6), confirming that the modification of the mix design does not affect the mechanical properties consistently.

Table 7. Flow value and R_c of the original and modified UNIVPM mortar mix.

MORTAR	CODE	FLOW VALUE (MM)	R _c (MPA)
Reference UNIVPM mortar	REF	116	4.4 ± 0.0
2% superplasticizer	2% SP	118	5.0 ± 0.0
1.5% cellulose fibers	1.5% CEL	115	3.5 ± 0.2

2.5% CaO	2.5% CaO	118	3.8 ± 0.1
5% CaO	5% CaO	116	3.9 ± 0.3

During the casting day, the five optimized mortars were spread on the hemp panel were the hemp-based mortar substrate (Rasante per LHP) was previously applied. After one month, the surfaces of the different mortars were visually analysed to evaluate the appearance of cracks (Figure 53). After 28 days of curing, the mortars showing diffuse cracks were the reference, as previously found, the 1.5% CEL mortar, since it was prepared with additional water to reach the same consistence of the reference one, and the 2.5% CaO mortar, probably because of the reduced amount of expansive agent. Indeed, the mortars that remained unaltered were the one prepared with 1.5% SP, which has required less water to reach the same stiff workability (thus less water that can evaporate was present inside the mix), and the one containing 5% CaO, giving the beneficial expansion of the calcium oxide, which counteracted the drying shrinkage. For this reason, the mortar composition chosen for the application in the Italian pilot was the one with the addition of 5% by hydraulic lime mass of CaO.

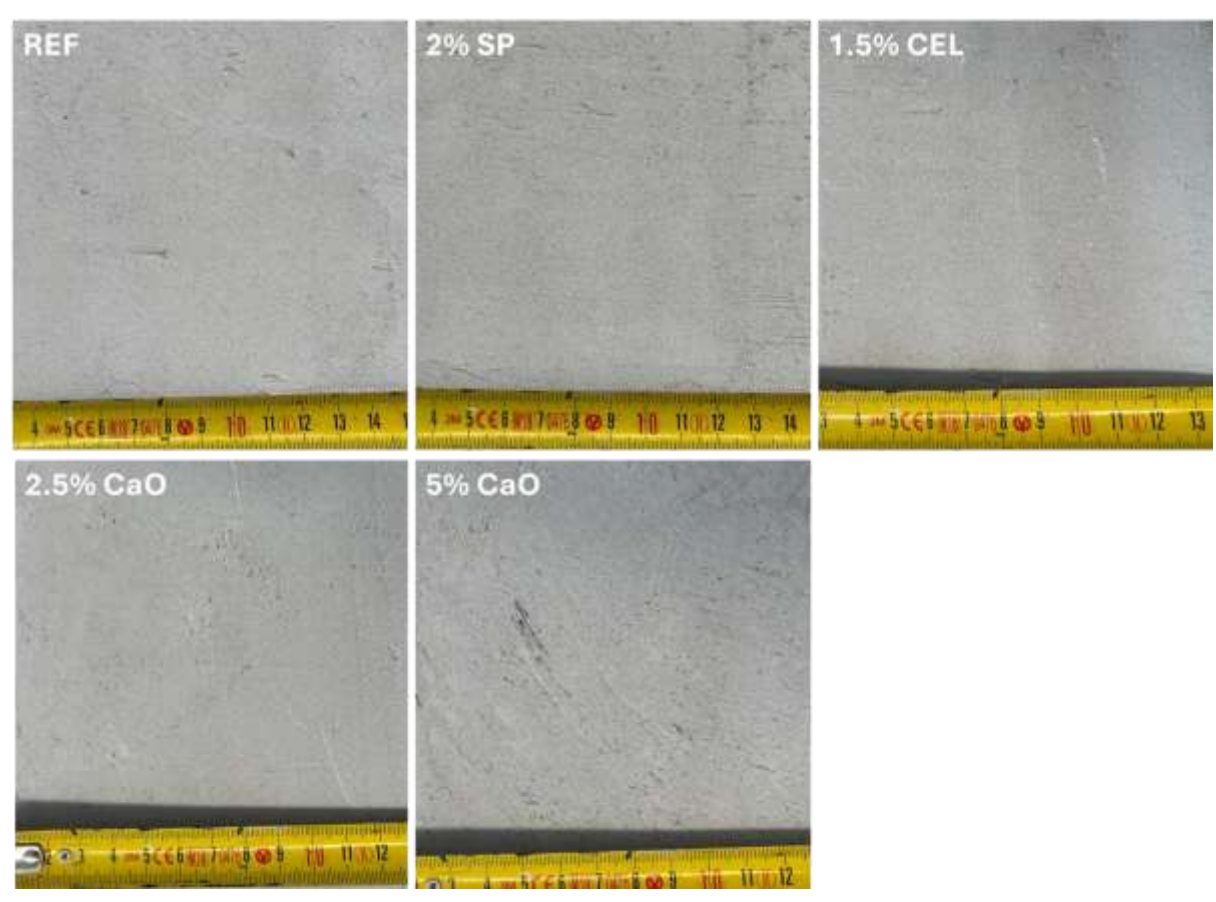


Figure 53. Visual aspect of mortars applied on natural-based panel and substrate after 28 days of curing (picture courtesy of UNIVPM).

5.3. PREPARATION OF THE ITALIAN PILOT

The innovative multilayer system based on hemp panel, hemp-based mortar substrate and the optimized multifunctional mortar (containing 5% of CaO) will be installed in one of the two twin rooms

selected in the ex-Carmelitane building (Figure 37). This innovative system will be applied at direct contact with the existing external wall in Room 2 (Figure 38). As reference, also the commercial system will be applied in the other twin room, namely Room 1 (Figure 38), at direct contact with the existing external wall. These two systems will be compared in terms of thermo-hygrometrical properties by ENEA.

ENEA has purchased 4 sensors for thermo-hygrometric monitoring (Figure 54). The sensor has a relative humidity measurement range: 0÷100% - Temperature measurement range: from -40 to +80°C. Thermo-hygrometric sensors will be installed inside the walls of the two rooms (Figure 37). Two sensors will be installed, one on the external wall and the other one on the internal wall to monitor the thermo-hygrometric behavior of the wall during the time. Figure 55 shows the installation diagram of the thermo-hygrometric sensors on the insulated walls made of XPS (red) and lime hemp (green).



Figure 54 Thermo-hygrometric sensor

The sensor network has been operationally tested and synchronized with the central system for remote management of continuous data collection and in continuous FTP.

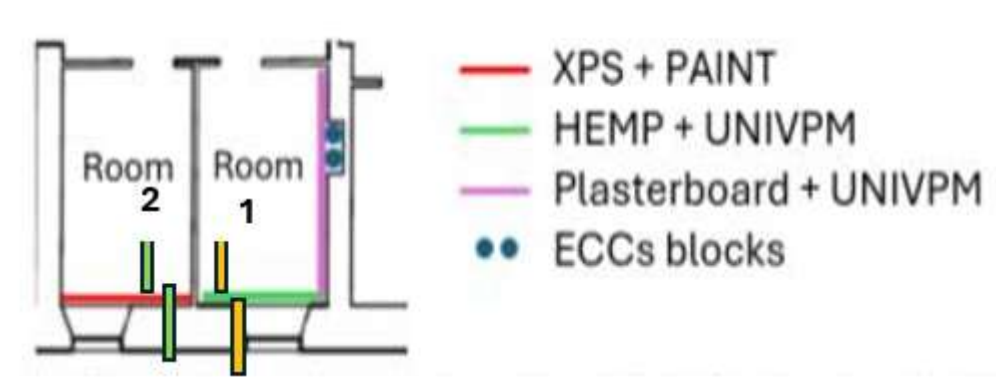


Figure 55 Position of the thermo-hygrometric sensors on the wall

The monitoring system also includes the use of an external control unit (Figure 56) for measuring weather parameters, equipped with an outdoor temperature and relative humidity probe with a relative humidity measurement range: 0÷100% - Temperature measurement range: from -40 to +80°C.



Figure 56 External control unit for weather monitoring

The innovative multifunctional mortar will be also applied to the existing internal wall in Room 2, previously covered by plasterboard and a hydraulic lime-based mortar substrate (Calce Storica by Diasen S.r.l., Sassoferrato (AN), Italy, https://www.diasen.com/) already used in a previous experimental campaign (Giosuè, Czerwinska, et al.), which proved the good thermo-hygrometric and depolluting properties of the UNIVPM patented mortar at a pilot scale (TRL 6). Indeed, in the MULTICLIMACT project the efficiency of the patented mortar will be tested in a real working environment to scale up the technology to TRL 7. The UNIVPM multifunctional mortar will cover a surface area of 3.7 m x 3.3 m, as shown in Figure 57. Then, several parameters will be monitored, comparing the results between Room 1 (reference indoor environment) and Room 2 (innovative indoor environment). In details, both environmental (T, RH, CO₂, PMs and VOCs concentration) and physiological parameters (heart rate, blood saturation, skin temperature, etc.) will be acquired by specific multidomain sensors integrated into the LIS' monitoring system. All these data will be exploited for indoor comfort assessment and definition of synthetic indices related to health and wellbeing (within the framework of T11.1 "Demonstration of the MULTICLIMACT framework at the building scale" and T15.1 "Deployment of the MULTICLIMACT framework at the building scale"). The followup of these activities will be then reported in the related deliverables.

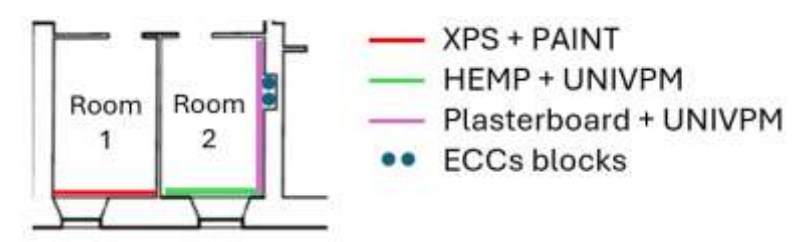


Figure 57. Scheme of positioning of the different innovative/reference systems (picture courtesy of UNIVPM).

6. DEVIATIONS TO THE PLAN

No deviations to the plan have to be reported.

7. OUTPUTS FOR OTHER WPS

The solutions developed within T9.3 will be deployed and validated in the upcoming project phases, namely:

- ECCs and multifunctional mortar are being deployed in the Italian demonstrator. They are being further tested within the framework of T11.1 (Develop and test phase) and will be demonstrated within the framework of T15.1 (Demonstration phase).
 - The low-temperature heating solution developed for the Latvian demonstrator is currently in the preliminary design phase for deployment. This design will serve as the basis for the upcoming BIM model. The system will be further tested and fine-tuned within the framework of T11.4 and T15.4.

8. CONCLUSION

Deliverable D9.3 focused on the development of resilience-oriented materials and HVAC technologies to support MULTICLIMACT actions in the built environment at multiple scales, with a strong emphasis on application at the building level.

All the activities foreseen in T9.3 have been successfully completed; the innovative solutions (materials and HVAC system) have been developed and are being (or will be) deployed in Italian and Latvian demos for their demonstration in real-scale environments.

In the Latvian pilot, KTH and Uponor jointly led the development of an integrated low-temperature heating system tailored to the Riga Central Market. Uponor developed the preliminary system design, including circuit and manifold layout, component specifications, and the bill of quantities. This design will serve as the foundation for the upcoming new BIM model. KTH contributed with comprehensive energy and resilience analyses, including thermal balance assessments and dynamic simulations under extreme weather scenarios (cold waves and heat waves). The main work carried out by KTH and Uponor focused on defining a future-proof, renewable-based HVAC concept built around five key components: a building-integrated photovoltaic system, a reversible heat pump, the district heating network, a low-temperature substation, and a combined low-temperature heating/high-temperature cooling distribution system using the Uponor underfloor heating network.

These contributions provide a robust foundation for climate-resilient HVAC retrofits in heritage buildings and demonstrate the applicability of integrated renewable-based solutions.

The results of tests conducted at laboratory scale for both ECCs and multifunctional mortar are promising, and the solutions are ready to be deployed in the Italian pilot. UNIVPM has already started the positioning of the components at "Le Carmelitane"building; the monitoring system for the demonstration phase (developed in close collaboration with the activities performed within the framework of T10.2 and T8.5) will be installed in early September, in close collaboration with T11.1. Hence, also the experimental campaign involving human subjects for the assessment of indoor multidomain comfort will start (T11.1, to be continued in T15.1).

9. LITERATURE /REFERENCES

- European Union. 2024. "Directive (EU) 2024/1275 of the European Parliament and of the Council of 24 April 2024 on the Energy Performance of Buildings." Official Journal of the European Union. Vol. 1275
- Falana, Justina, Robert Osei-Kyei, and Vivian WY Tam. 2024. "Towards Achieving a Net Zero Carbon Building: A Review of Key Stakeholders and Their Roles in Net Zero Carbon Building Whole Life Cycle." Journal of Building Engineering 82 (April 2023): 108223. https://doi.org/10.1016/j.jobe.2023.108223.
- Liu, Xiaohua, Tao Zhang, Haida Tang, and Yi Jiang. 2017. "IEA EBC Annex 59: High Temperature Cooling and Low Temperature Heating in Buildings." Energy and Buildings 145:267-75. https://doi.org/10.1016/j.enbuild.2017.04.036.
- Quirosa, Gonzalo, Miguel Torres, V. M. Soltero, and Ricardo Chacartegui. 2022. "Analysis of an Ultra-Low Temperature District Heating and Cooling as a Storage System for Renewable Integration." Applied Thermal Engineering 216 (March): 119052. https://doi.org/10.1016/j.applthermaleng.2022.119052.
- Zhao, Bin, Qingdong Xuan, Chengfeng Xu, Mingke Hu, Yousef N. Dabwan, and Gang Pei. 2023. "Considerations of Passive Radiative Cooling." Renewable Energy 219 (P2): 119486. https://doi.org/10.1016/j.renene.2023.119486.
- Bahri, Mitra, et al. "Removal Performance of Formaldehyde by Ceiling Tiles as Sorptive Passive Panels." Building and Environment, vol. 160, Elsevier, 2019, p. 106172, doi:10.1016/j.buildenv.2019.106172.
- Cosoli, Gloria, et al. "Electrical Resistivity and Electrical Impedance Measurement in Mortar and Concrete Elements: A Systematic Review." Applied Sciences, vol. 10, no. 24, 2020, p. 9152, doi:10.3390/app10249152.
- EN 1015-11:1999/A1:2006 Methods of Test for Mortar for Masonry Part 11: Determination of Flexural and Compressive Strength of Hardened Mortar. European Committee for Standardization, 2006.
- EN 1015-3:1999/A2:2006 Methods of Test for Mortar for Masonry Part 3: Determination of Consistence of Fresh Mortar (by Flow Table). European Committee for Standardization, 2006.
- EN 1015-6:1998/A1:2006 Methods of Test for Mortar for Masonry Part 6: Determination of Bulk Density of Fresh Mortar. European Committee for Standardization, 2006.
- EN 12504-4:2004 Testing Concrete in Structures Part 4: Determination of Ultrasonic Pulse Velocity. European Committee for Standardization, 2004.
- Gayakwad, Himanshi, and Jothi Saravanan Thiyagarajan. "Structural Damage Detection through EMI and Wave Propagation Techniques Using Embedded PZT Smart Sensing Units." Sensors 2022, Vol. 22, Page 2296, vol. 22, no. 6, Multidisciplinary Digital Publishing Institute, Mar. 2022, p. 2296, doi:10.3390/S22062296.
- Giosuè, Chiara, Mattia Pierpaoli, Alessandra Mobili, et al. "Influence of Binders and Lightweight Aggregates on the Properties of Cementitious Mortars: From Traditional Requirements to Indoor Air Quality Improvement." Materials, vol. 10, no. 8, 2017, p. 978, doi:10.3390/ma10080978.
- Giosuè, Chiara, Natalia Czerwinska, et al. "Innovative Multifunctional Finish for the Improvement of Indoor Air Quality: Performance at Laboratory and Pilot Scale." Building and Environment, vol. 273, 2025, p. 112697, doi:10.1016/j.buildenv.2025.112697.
- Giosuè, Chiara, Mattia Pierpaoli, Barbara Citterio, et al. "Properties of an Innovative Multi-Functional Finish for the Improvement of Indoor Air Quality." Building and Environment, vol. 233, 2023, p. 110091, doi:10.1016/j.buildenv.2023.110091.
- González-Martín, Javier, et al. "A State-of-the-Art Review on Indoor Air Pollution and Strategies for



- D9.3 Cutting-edge, evolutive, self-sensing and multi-functional materials and technologies for improving the resilience of buildings, including cultural heritage development for the application to real demo
 - Indoor Air Pollution Control." Chemosphere, vol. 262, 2021, p. 128376, doi:10.1016/j.chemosphere.2020.128376.
- Klun, Mateja, et al. "On the Application of Laser Vibrometry to Perform Structural Health Monitoring in Non-Stationary Conditions of a Hydropower Dam." Sensors 2019, Vol. 19, Page 3811, vol. 19, no. 17, Multidisciplinary Digital Publishing Institute, Sept. 2019, p. 3811, doi:10.3390/S19173811.
- Kunkel, Donna A., et al. "Passive Reduction of Human Exposure to Indoor Ozone." Building and Environment, vol. 45, no. 2, Elsevier Ltd, 2010, pp. 445-52, doi:10.1016/j.buildenv.2009.06.024.
- Li, Zhenkun, et al. "Drive-by Bridge Damage Detection Using Mel-Frequency Cepstral Coefficients and Support Vector Machine." Structural Health Monitoring, vol. 22, no. 5, 2023, pp. 3302-19, doi:10.1177/14759217221150932.
- Mazhoud, Brahim, et al. "Hygric and Thermal Properties of Hemp-Lime Plasters." Building and Environment, vol. 96, Elsevier Ltd, 2016, pp. 206-16, doi:10.1016/j.buildenv.2015.11.013.
- Mobili, Alessandra, et al. "Biochar and Recycled Carbon Fibres as Additions for Low-Resistive Cement-Based Composites Exposed to Accelerated Degradation." Construction and Building Materials, vol. 376, Elsevier Ltd, 2023, p. 131051, doi:10.1016/j.conbuildmat.2023.131051.
- Ozelim, Luan Carlos de Sena Monteiro, et al. "Structural Health Monitoring of Dams Based on Acoustic Monitoring, Deep Neural Networks, Fuzzy Logic and a CUSUM Control Algorithm." Sensors 2022, Vol. 22, Page 2482, vol. 22, no. 7, Multidisciplinary Digital Publishing Institute, Mar. 2022, p. 2482, doi:10.3390/S22072482.
- Pierpaoli, Mattia, et al. "Appraisal of a Hybrid Air Cleaning Process." Environmental Science and Pollution Research, vol. 24, 2017, pp. 12638-45, doi:10.1007/s11356-016-7880-x.
- Ren, Qiang, et al. "Cement-Based Composite with Humidity Adsorption and Formaldehyde Removal Functions as an Indoor Wall Material." Construction and Building Materials, vol. 247, Elsevier Ltd, 2020, p. 118610, doi:10.1016/j.conbuildmat.2020.118610.
- Sofi, A., et al. "Structural Health Monitoring Using Wireless Smart Sensor Network An Overview." Mechanical Systems and Signal Processing, vol. 163, Academic Press, Jan. 2022, p. 108113, doi:10.1016/J.YMSSP.2021.108113.
- Tittarelli, Francesca, et al. Sistemi Innovativi per Il Monitoraggio Della Durabilità Delle Infrastrutture. 2020, https://www.ingenio-web.it/articoli/sistemi-innovativi-per-il-monitoraggio-continuo-della-durabilita-delle-infrastrutture-in-calcestruzzo/.
- Wen, Sihai, and D. D. L. Chung. "Piezoresistivity in Continuous Carbon Fiber Cement-Matrix Composite." Cement and Concrete Research, vol. 29, no. 3, 1999, pp. 445-49, doi:10.1016/S0008-8846(98)00211-7.
- Wenner, Frank. "A Method for Measuring Earth Resistivity." Journal of the Washington Academy of Sciences, vol. 5, no. 16, 1915, pp. 561-63, doi:10.6028/bulletin.282.
- Zuraimi, M. S., et al. "Performance of Sorption- and Photocatalytic Oxidation-Based Indoor Passive Panel Technologies." Building and Environment, vol. 135, 2018, pp. 85-93, doi:10.1016/j.buildenv.2018.03.004.



